

RECLAMATION

Managing Water in the West

Desalination and Water Purification Research
and Development Program Report No. 212

Improved Energy Efficiency of Electrodialysis Desalination and Separation: Development of Percolating Network Nanocomposite Ion-Exchange Membranes for High Conductivity



U.S. Department of the Interior
Bureau of Reclamation
Technical Service Center
Denver, Colorado

February 2019

REPORT DOCUMENTATION PAGE*Form Approved
OMB No. 0704-0188*

The public reporting burden for this collection of information is estimated to average 1 hour per response, including the time for reviewing instructions, searching existing data sources, gathering and maintaining the data needed, and completing and reviewing the collection of information. Send comments regarding this burden estimate or any other aspect of this collection of information, including suggestions for reducing the burden, to Department of Defense, Washington Headquarters Services, Directorate for Information Operations and Reports (0704-0188), 1215 Jefferson Davis Highway, Suite 1204, Arlington, VA 22202-4302. Respondents should be aware that notwithstanding any other provision of law, no person shall be subject to any penalty for failing to comply with a collection of information if it does not display a currently valid OMB control number.

PLEASE DO NOT RETURN YOUR FORM TO THE ABOVE ADDRESS.

1. REPORT DATE (DD-MM-YYYY) February 25, 2019	2. REPORT TYPE Final	3. DATES COVERED (From - To) June 1, 2017 – December 31, 2018
4. TITLE AND SUBTITLE Improved Energy Efficiency of Electrodialysis Desalination and Separation: Development of Percolating Network Nanocomposite Ion-Exchange Membranes for High Conductivity	5a. CONTRACT NUMBER Agreement No. R16AC00124	
	5b. GRANT NUMBER	
	5c. PROGRAM ELEMENT NUMBER	
6. AUTHOR(S) Ngai Yin Yip, Ph.D. Assistant Professor Department of Earth and Environmental Engineering Columbia University	5d. PROJECT NUMBER	
	5e. TASK NUMBER	
	5f. WORK UNIT NUMBER	
7. PERFORMING ORGANIZATION NAME(S) AND ADDRESS(ES) The Trustees of Columbia University 615 West 131st Street Room 254, Mail Code 8725 New York, NY 10027-7922	8. PERFORMING ORGANIZATION REPORT NUMBER	
9. SPONSORING/MONITORING AGENCY NAME(S) AND ADDRESS(ES) Bureau of Reclamation U.S. Department of the Interior Denver Federal Center PO Box 25007, Denver, CO 80225-0007	10. SPONSOR/MONITOR'S ACRONYM(S) Reclamation	
	11. SPONSOR/MONITOR'S REPORT NUMBER(S) DWPR Report No. 212	
12. DISTRIBUTION/AVAILABILITY STATEMENT Available from the National Technical Information Service, Operations Division, 5285 Port Royal Road, Springfield VA 22161		
13. SUPPLEMENTARY NOTES Online at https://www.usbr.gov/research/dwpr/DWPR_Reports.html		
14. ABSTRACT		

Nanocomposite cation exchange membranes have been fabricated by incorporating sulfonated carbon nanotubes into sulfonated poly(p-phenylene oxide) polymer matrix (0-20 w/w%). The percolating network of carbon nanotubes can advantageously lower the intrinsic resistivity of the nanocomposite membrane while the charged functional moieties intensifies the Donnan exclusion effect, thus sustaining a high permselectivity. Nanocomposite IEMs exhibit improved conductivity while maintaining permselectivity. Intrinsic resistivity, inverse of conductivity, decreases 25 to 29 percent, with 20 percent incorporation of sCNT. Enhancement in conductivity is more pronounced for membranes with lower swelling degree. The nanocomposite fabrication strategy can advance the permselectivity-conductivity tradeoff to obtain IEMs with improved performance. The electro dialysis desalination of brackish water to drinking water standards (1,000 ppm TDS) has been demonstrated with the fabricated nanocomposite membranes. Projected energy savings of about 13.3 to 15.8 percent for brackish water desalination is achievable with nanocomposite membranes. This study demonstrates the rational use of nanomaterials as a promising platform to advance the conductivity-permselectivity trade-off governing conventional IEMs.

15. SUBJECT TERMS

Ion-exchange membranes, conductivity-permselectivity tradeoff, carbon nanotubes, nanocomposite, chemical functionalization

16. SECURITY CLASSIFICATION OF:			17. LIMITATION OF ABSTRACT	18. NUMBER OF PAGES	19a. NAME OF RESPONSIBLE PERSON Miguel Arias-Paic, Environmental Engineer
a. REPORT U	b. ABSTRACT U	THIS PAGE U			19b. TELEPHONE NUMBER (Include area code) 303-445-2132

**Desalination and Water Purification Research
and Development Program Report No. 212**

Improved Energy Efficiency of Electrodialysis Desalination and Separation: Development of Percolating Network Nanocomposite Ion- Exchange Membranes for High Conductivity

**Prepared for the Bureau of Reclamation Under
Agreement No. R16AC00124**

by

Ngai Yin Yip, Ph.D.
Assistant Professor
Department of Earth and Environmental Engineering
Columbia University

Mission Statements

The U.S. Department of the Interior protects America's natural resources and heritage, honors our cultures and tribal communities, and supplies the energy to power our future.

The mission of the Bureau of Reclamation is to manage, develop, and protect water and related resources in an environmentally and economically sound manner in the interest of the American public.

Disclaimer

The views, analysis, recommendations, and conclusions in this report are those of the authors and do not represent official or unofficial policies or opinions of the United States Government, and the United States takes no position with regard to any findings, conclusions, or recommendations made. As such, mention of trade names or commercial products does not constitute their endorsement by the United States Government.

Acknowledgements

The author acknowledges The Desalination and Water Purification Research and Development Program, Bureau of Reclamation for sponsorship of the research.

Acronyms and Abbreviations

AEM	anion exchange membrane
ASR	area specific resistance
ASC	area specific conductance
CEM	cation exchange membrane
CE	current efficiency
DMSO	dimethyl sulfoxide
ED	electrodialysis
HC	high concentration
HNO ₃	nitric acid
H ₂ SO ₄	sulfuric acid
IEC	ion-exchange capacity
IEM	ion-exchange membrane
LC	low concentration
pCNT	pristine carbon nanotube
PPO	poly(p-phenylene oxide)
PTFE	poly(1,1,2,2-tetrafluoroethylene)
RED	reverse electrodialysis
RO	reverse osmosis
sCNT	sulfonated carbon nanotube
SOCl ₂	thionyl chloride

TDS	total dissolved solids
TEA	triethylamine
THF	tetrahydrofuran
XPS	X-ray photoelectron spectroscopy
a	activity
b	distance between fixed charges on the polymer chain
c	molar concentration
$c_{\text{fix}}^{\text{m}}$	fixed charge density of membrane
\bar{c}^{m}	concentration normalized by unit volume of solution sorbed by membrane (excluding polymer volume)
e	elementary charge
f_{w}	volume fraction of water
k_{B}	Boltzmann constant
l	membrane thickness
\hat{i}	current density
\hat{i}_{tot}	net current density
t	transport number
z	valence of the ion
D	diffusion coefficient
F	Faraday constant
J	mass flux

K	partition coefficient
P	hydrostatic pressure
R_g	gas constant
T	absolute temperature
\bar{V}	partial molar volume
ΔV^m	external membrane potential drop including Donnan potentials at membrane-solution interface
Z	ratio of z_{co}/z_{ct}
α	permselectivity measured by transport number
α_{app}	apparent permselectivity measured by open-circuit voltage
β	membrane activity correction factor for Nernst-Planck equation, $1 + c_i^m \left(d \ln \gamma_i^m / dc_i^m \right)$
γ	activity coefficient
γ_{\pm}^s	salt activity coefficient in bulk solution
ϵ_0	vacuum permittivity
ϵ_t	solvent dielectric constant
λ_B	Bjerrum length
$\bar{\mu}$	electrochemical potential
μ	chemical potential
μ^0	standard state chemical potential

ν	dissociation number
ξ	dimensionless linear charge density of the polymer
ρ	resistivity
ρ_p	mass density of dry polymer
σ	conductivity
τ	tortuosity
φ	electric potential
$\Delta\varphi_{\text{Donnan}}$	Donnan potential
$\Delta\varphi^m$	internal membrane potential drop excluding Donnan potentials at membrane-solution interface
χ	ratio of co-ion charge to fixed charge density, $z_{\text{co}}c_{\text{co}}^m/c_{\text{fix}}^m$
i	mass species
s	bulk solution phase
m	membrane phase
ct	counterion
co	co-ion
w	water
p	polymer

Measurements

cm^3/g	Gram per cubic centimeter
eq/L	Equivalents per liter
eV	electronvolt
g/mL	Grams per milliliter
mol/L	Moles per liter
mA	milliamps
mA/cm^2	Milliamps per square centimeter
meq/g	Milliequivalents per gram
mg	milligram
μm	micrometer
mL	Milliliter
mmHg	Millimeters of mercury (to measure pressure)
nm	nanometer
ppm	Parts per million
S/cm^2	Siemens per square centimeter
S/m	Siemens per meter
sA/mol	second Ampere per mole (unit for Faraday constant)
v\%	Volume percent
w/w\%	Weight percent
Ωcm^2	ρεσιστανχε αρεα σθυαρε (υνιτ φορ αρεα σπεχιφιχ ρεσιστανχε)

wt.% weight percent

Table of Contents

Executive Summary	21
1 Introduction.....	23
1.1 Background.....	23
1.2 Project Needs	24
1.3 Project Objectives	26
2 Transport model for ion exchange membranes.....	28
2.1 Transport model development	28
2.2 Influence of operating parameters	28
2.2.1 Operating electric potential.....	29
2.2.2 External solution concentrations.....	30
2.3 Influence of structural properties	32
2.3.1 Ion exchange capacity.....	32
2.3.2 Swelling degree.....	34
2.3.3 Membrane thickness	36
2.4 Implications.....	37
3 Carbon nanotubes functionalization and characterization	38
3.1 Materials and Methods.....	38
3.1.1 Materials	38
3.1.2 Synthesis of sulfonated CNT	39
3.1.3 Preparation of sulfonated CNT for characterization.....	42
3.2 Characteristics of functionalization CNT	42
3.2.1 Stabilized sulfonation result of Method 1	42
3.2.2 Dispersion of sCNT in polar solvents.....	44
3.2.3 Sulfonation result of Method 2	45
4 Nanocomposite ion exchange membrane fabrication and characterization	48
4.1 Nanocomposite IEM fabrication.....	48
4.1.1 Polymer functionalization.....	48
4.1.2 Preparation of casting solutions	48

4.1.3	Membrane casting.....	48
4.2	IEM characterization.....	49
4.2.1	Ion-exchange capacity	49
4.2.2	Swelling degree.....	49
4.2.3	Membrane intrinsic resistivity/conductivity	50
4.2.4	Membrane permselectivity.....	51
4.2.5	Scanning electron microscopy imaging	51
4.3	Results and discussion	52
4.3.1	Nanocomposite with lab-functionalized sCNTs	52
4.3.2	Nanocomposite with commercial sCNTs	53
4.3.3	Morphology of nanocomposite IEMs	54
5	Impacts of sCNT incorporation on the conductivity-permselectivity trade-off.....	61
5.1	Resistivity reduction from incorporation of sCNT	61
5.2	Advancing conductivity-permselectivity trade-off.....	62
6	Electrodialysis stack test and performance assessment	63
6.1	Methods.....	63
6.2	Nanocomposite IEM desalination.....	64
6.3	Desalination results with commercial IEM.....	65
6.4	Energy requirement assessment.....	66
7	Concluding remarks	68
7.1	Summary of project outcomes	68
7.2	Recommended next steps.....	68
7.3	Research products	69
7.3.1	Publications.....	69
7.3.2	Conference presentations	69
	Appendix – Model Development.....	71
	References.....	80

Figures

Figure 1-1. Schematic of ED, with the arrows indicating the direction of cation (+) and anion (-) permeation. Repeating pairs of CEMs and AEMs selectively allow the permeation of counterions while rejecting co-ions. Note that only one IEM pair and the end electrodes are shown. A reversible redox couple is circulated at the end electrodes to convert between the ionic current and the electric current.	24
Figure 1-2. Schematic of a cation exchange membrane with fixed negative charges within the polymer matrix. Because of charge exclusion, co-ions (anions) are almost entirely excluded from the membrane matrix and, therefore, the CEM allows selective passage of counterions (cations), as indicated by the directional arrow.	25
Figure 1-3. Selectivity of IEMs, presented as $1/(1-\alpha)$, as a function of conductivity, σ . The negative slope of the green line represents the empirical conductivity-permselectivity trade-off relation of IEMs, in which an increase in conductivity is accompanied by a decrease in permselectivity. Blue squares and red circles denote commercially available and laboratory-fabricated IEMs, respectively (Długołęcki et al. 2008a, Güler et al. 2013).	26
Figure 2-1. Current efficiency (CE; green square, left vertical axis) and area specific resistance (ASR; red triangles, right vertical axis) as a function of external electric potential difference across the membrane, ΔV^m for ED desalination of simulated brackish water at 200×10^{-3} mol/L NaCl to produce product water of 1,000 ppm TDS ($= 17 \times 10^{-3}$ mol/L NaCl).	29
Figure 2-2. CE and ASC (vertical and horizontal axes, respectively) with $c^{s,HC}$ increasing from 0.1 to 1.2 mol/L NaCl in ED (data point labels), representing desalination of brackish water to brine twice the concentration of seawater.	30
Figure 2-3. Contour plot of A) apparent permselectivity and B) conductivity as functions of HC and LC bulk solution NaCl concentrations (horizontal and vertical axes, respectively).	31
Figure 2-4. A) Relative concentration of counter- to co-ions, as a function of bulk solution concentration for different membrane fixed charge densities. Note that both axes are on logarithmic scale. B) Permselectivity, α , and conductivity, σ , with increasing membrane ion-exchange capacity for ED.	33
Figure 2-5. A) Water volume fraction, f_w , membrane tortuosity, τ (primary and secondary left vertical axes: blue triangle and violet diamond symbols, respectively), and fixed charge density, c_{fix}^m (right vertical axis, green pentagon symbols), as a function of swelling degree. B) Permselectivity, α , and conductivity, σ , with increasing swelling degree.	35

Figure 2-6. Permselectivity (α ; dotted symbols, left vertical axis) and ASC (crossed symbols, right vertical axis) as a function of membrane thickness, l	37
Figure 3-1. Schematic of the acetyl sulfuric acid method (Wei et al. 2015).	39
Figure 3-2. Experimental procedures of the acetyl sulfuric acid method: A) Concentrated sulfuric acid and acetic anhydride are stirred in an ice-water bath to generate acetyl sulfuric acid; B) pCNT is dispersed in the acid mixture by sonication in an ice-water bath (the ice-water bath prevents acetyl sulfuric acid from being converted to sulfoacetic acid (Moulder et al.), which is undesirable for subsequent reactions); C) the mixture was stirred at 80°C to allow acetyl sulfuric acid to react with C-H defects on pCNT; D) product sCNT.....	40
Figure 3-3. Schematic the acyl chloride sulfonation method (Yun et al. 2011). ...	41
Figure 3-4. Experimental procedures of the acyl chloride sulfonation method: A) pCNT is stirred under reflux in H ₂ SO ₄ and HNO ₃ (3:1 by v%) at 80°C; B) CNT-COOH is stirred under reflux in SOCl ₂ at 70° C; C) CNT-COCl is stirred under reflux in aminomethanesulfonic acid solution with addition of sodium hydroxide at 80° C; D) product sCNT.	41
Figure 3-5. sCNT powder on indium foil substrate for XPS analysis.	42
Figure 3-6. Full XPS spectrum of pCNT (gray) and sCNT using method 1 (red).	42
Figure 3-7. XPS detailed spectra of pCNT (left column): a) C1s spectrum, c) O1s spectrum, e) S2p spectrum; sCNT using method 1 (right column): b) C1s spectrum, d) O1s spectrum, f) S2p spectrum.	43
Figure 3-8. Dispersion test of sCNT and pCNT. A) 5 mg of pCNT (left) and sCNT (right) in 5 mL ultrapure water with 10-minute sonication; B) 10 days after sonication, pCNT (left) agglomerated and settled, while sCNT maintained good dispersion; C) 5 mg of pCNT (left) and sCNT (right) in 5 mL DMSO with 3-minute sonication; D) 10 hours after sonication, pCNT aggregates settled at the bottom while sCNT was still well dispersed.....	45
Figure 3-9. Full XPS spectrum of sCNT using method 2.....	46
Figure 3-10. XPS detailed spectra of sCNT using method 2: a) C1s spectrum; b) O1s spectrum; c) S2p spectrum; d) N1s spectrum.....	46
Figure 4-1. Experimental procedures of sCNT nanocomposite IEM fabrication: A) Sulfonated PPO polymer; B) Casting solution (sPPO and sCNTs in DMSO); C) spreading casting solution into a thin film with a casting knife; D) Nanocomposite cation exchange membrane.....	49
Figure 4-2. Experimental methods for membrane resistance/conductance measurements: A) Schematic of the four-electrode test; B) Membrane resistance	

test cell; C) Voltage response for different constant current steps; D) Representative plot of membrane resistance calculation.	50
Figure 4-3. Schematic diagram of permselectivity test.	51
Figure 4-4. l , ion-exchange capacity, swelling degree, ASR, ρ and α of the fabricated membranes (with lab-functionalized sCNTs).	52
Figure 4-5. Intrinsic resistivity, ρ , as a function of weight percent of lab-functionalized sCNTs in IEM; and permselectivity, α , which is effectively independent of sCNT addition.	53
Figure 4-6. l , ion-exchange capacity, swelling degree, ASR, ρ and α of the fabricated membranes (with commercial sCNTs).	54
Figure 4-7. Intrinsic resistivity, ρ , as a function of weight percent of commercial sCNTs in IEM; and permselectivity, α , which is basically independent on sCNT addition.	54
Figure 4-8. 0 w/w% sCNTs IEM cross-section: A) $\times 500$ magnification, B) $\times 10,000$ magnification, C) $\times 50,000$ magnification	55
Figure 4-9. 0 w/w% sCNTs IEM surface: A) $\times 500$ magnitude, B) $\times 10,000$ magnitude, C) $\times 50,000$ magnitude	55
Figure 4-10. 10 w/w% sCNTs IEM cross-section: A) $\times 500$ magnification, B) $\times 10,000$ magnification, C) $\times 50,000$ magnification	56
Figure 4-11. 10 w/w% sCNTs IEM surface, top view: A) $\times 1000$ magnification, B) $\times 10,000$ magnification, C) $\times 50,000$ magnification	57
Figure 4-12. 10 w/w% sCNTs IEM surface, bottom view: A) $\times 500$ magnification, B) $\times 10,000$ magnification, C) $\times 50,000$ magnification	57
Figure 4-13. 20 w/w% sCNTs IEM cross-section: A) $\times 500$ magnification, B) $\times 10,000$ magnification, C) $\times 50,000$ magnification	58
Figure 4-14. 20 w/w% sCNTs IEM surface, top view: A) $\times 1000$ magnification, B) $\times 10,000$ magnification, C) $\times 50,000$ magnification	59
Figure 4-15. 20 w/w% sCNTs IEM surface, bottom view: A) $\times 1000$ magnification, B) $\times 10,000$ magnification, C) $\times 50,000$ magnification	59
Figure 5-1. Intrinsic resistivity, ρ , as a function of swelling degree, for sCNT-incorporated and control membranes.	61
Figure 5-2. Permselectivity as a function of conductivity for 0 and 20 % sCNT in sPPO IEM.	62
Figure 5-3. Schematic of posited ion transport in pristine and nanocomposite IEM.	63

Figure 6-1. Design of the ED stack: A) operation of the ED stack, B) schematic of the stack, with the arrows indicating the direction of electric current or cation (+) and anion (-) permeation. CEMs and AEM separate diluate (LC) and concentrate (HC) flow channels. The electrode rinse solution is also circulated between electrode chambers (light gray chamber).....64

Figure 6-2. ED operation of IEM stack with 10 w/w% sCNT CEM. A) Concentration of diluate channel (LC) as a function of time, and B) stack voltage across two end electrodes.....65

Figure 6-3. ED operation of the IEM stack with commercial CEM. A) Concentration of diluate channel (LC) as a function of time, and B) stack voltage across two end electrodes.....66

Figure 6-4. Projected specific energy requirement of ED desalination with conventional and nanocomposite IEMs.67

Tables

Table 3-1. Atomic composition of pCNT and sCNT using method 1.44

Table 3-2. Atomic composition of pCNT and sCNT using method 2.47

Executive Summary

Motivation

Seawater desalination allows us to access the limitless water in the oceans to augment our potable water supplies but is energy-intensive even for the most efficient technology, reverse osmosis. Because of the lower salinity, brackish water desalination has a lower energy requirement. However, the disposal of concentrated brine from inland brackish water desalination poses considerable environmental challenges. At the same time, wastewater reuse, in which wastewater effluent that is typically discharged to the environment undergoes further treatment to reclaim the water, can alleviate some of the stress on our water supplies. In addition to water, nitrogen and phosphorus – essential components of agricultural fertilizers – can also be recovered from wastewater as a more sustainable approach to address our global food challenges. Both desalination and wastewater reuse are actively considered options to address the critical water issues facing the American Southwest. In order for desalination and wastewater reuse to be sustainable solutions to our water problems, the development of more efficient and effective technologies is needed.

Background

Electrodialysis (ED) is a membrane-based process that can desalinate seawater and brackish water and carry out charge-based separation to recover nutrients from waste streams. In ED, an electric potential is applied to alternating pairs of cation and anion exchange membranes to drive the permeation of counterions across the ion-exchange membranes (IEMs), retaining co-ions and water. Ions are removed from the feed stream flowing between the IEM pair while the adjacent compartment is concentrated. The charged-based separation enables ED to be used for selective ion removal. Nitrogen and phosphorus, as positively charged ammonium and negatively charged phosphate, respectively, can be selectively extracted from wastewater for reuse and, at the same time, treat the wastewater.

Problem Statement

A fundamental limitation of electrodialysis is the inherently low conductivity of conventional IEMs. The large contribution of the IEMs to the resistance of the ED stack results in high internal resistance in the electrodialysis circuit, consequently causing elevated ohmic losses that detrimentally lower the energy efficiency. Additionally, the low conductivity slows process kinetics by diminishing the ion flux. Membrane development efforts to lower the intrinsic resistivity of conventional polymeric IEMs also invariably decreased the membrane permselectivity, the discriminating ability of the membrane to selectively allow counterion passage while repelling co-ions. To advance IEMs beyond their current high-resistance drawback without sacrificing ion selectivity, innovative membranes that break away from the conductivity-permselectivity tradeoff are needed.

Approach

Nanocomposite IEMs with a percolating network of rationally functionalized one-dimensional nanomaterials can attain high intrinsic conductivity while preserving permselectivity. Because of the large aspect ratio and the nanoscale dimensions, a given amount of non-aggregated, one-dimensional nanomaterial, such as carbon nanotubes, can achieve several orders of magnitude greater dispersity than micro-scale fillers. Carbon nanotubes have been purposefully functionalized with sulfonic acid to confer desired properties to the nanomaterial. Rationally modified carbon nanotubes using sulfonic acid (–) to achieve a high charge density were dispersed in the polymer matrix during membrane fabrication to form a percolating network within the polymer thin-film.

Outcomes

Nanocomposite cation exchange membranes have been fabricated by incorporating sulfonated carbon nanotubes into sulfonated poly(p-phenylene oxide) polymer matrix (0-20 w/w%). The percolating network of carbon nanotubes can advantageously lower the intrinsic resistivity of the nanocomposite membrane while the charged functional moieties intensifies the Donnan exclusion effect, thus sustaining a high permselectivity. Nanocomposite IEMs exhibit improved conductivity while maintaining permselectivity. Intrinsic resistivity, inverse of conductivity, decreases 25 to 29 percent, with 20 percent incorporation of sCNT. Enhancement in conductivity is more pronounced for membranes with lower swelling degree. The nanocomposite fabrication strategy can advance the permselectivity-conductivity tradeoff to obtain IEMs with improved performance. The electrodialysis desalination of brackish water to drinking-water standards (1,000 ppm total dissolved solids [TDS]) has been demonstrated with fabricated nanocomposite membranes. Projected energy savings of about 13.3 to 15.8 percent for brackish water desalination is achievable with nanocomposite membranes. This study demonstrates the rational use of nanomaterials as a promising platform to advance the conductivity-permselectivity trade-off governing conventional IEMs.

1 Introduction

1.1 Background

Addressing our water challenges is one of the most pressing priorities for the 21st century (Bogardi et al. 2012, Rockström et al. 2009, Running 2012, Vorosmarty et al. 2010), an urgency echoed by the National Academy of Engineering's Grand Challenges (Perry et al. 2008). Approximately 35 percent of the world's population is living in water-stressed areas (Oki and Kanae 2006). In the United States, increasing human appropriation of freshwater resources presents a tangible limit to the sustainability of cities, agriculture, and ecosystems in the American West, where nearly 76 percent of streamflow in the Cadillac Desert region is currently appropriated (Sabo et al. 2010). To address the world's and the United States' daunting water challenges, it is imperative to advance the science and technology of water production and purification (Elimelech 2006, Shannon et al. 2008). Desalination can augment our water supply by tapping into the limitless reservoir of water in the oceans (Elimelech and Phillip 2011, Ghaffour et al. 2013) and brackish groundwater in non-coastal areas (Ghaffour et al. 2013). The promise of desalination to provide a secure supply of water can potentially address the water issues in the American Southwest (Cooley et al. 2012, Gleick 2010, MacDonald 2010).

Electrodialysis (ED) is a membrane-based technology that uses an electric current to separate charged ions from a saline stream to produce freshwater (Baker 2012, Mulder 1996, Sata 2004, Strathmann 2004a, Tanaka 2015). Ion-exchange membranes (IEMs) that selectively allow the passage of solute based on charge are employed in ED (Figure 1-1). An external electric potential is applied across a stack comprising repeating pairs of cation exchange membranes (CEM) and anion exchange membranes (AEM), with the saline feed stream flowing through each compartment channel between the membranes. The external potential drives the permeation of cations toward the cathode and the anions towards the anode. As the IEMs selectively allow the passage of counterions (i.e., cations for the negatively charged CEMs and anions for the positively charged AEMs), co-ions are retained while counterions permeate across the membranes into the adjacent channel. A reversible redox couple (e.g., $\text{Fe}^{2+}/\text{Fe}^{3+}$ or $[\text{Fe}(\text{CN})_6]^{4-}/[\text{Fe}(\text{CN})_6]^{3-}$) is circulated between the end electrodes to convert the ionic current to an electric current, thereby closing the circuit (Figure 1-1).

In ED desalination, the net transport of ions results in a decrease in the salt concentration of every other solution compartment, while the salt concentration of adjacent channels increases (Figure 1-1). Therefore, the saline feed solution (e.g., seawater or brackish groundwater) is separated into a desalinated product water

stream and a waste brine stream (Sadrzadeh and Mohammadi 2008, Strathmann 2010). Alternatively, for nutrient recovery in which ammonium or phosphate is the desired product, the wastewater effluent can be paired with a working solution to collect the N or P nutrients (concentrated stream), at the same time treating the wastewater by removing the nutrients (diluted stream) (Mondor et al. 2008, Zhang et al. 2013).

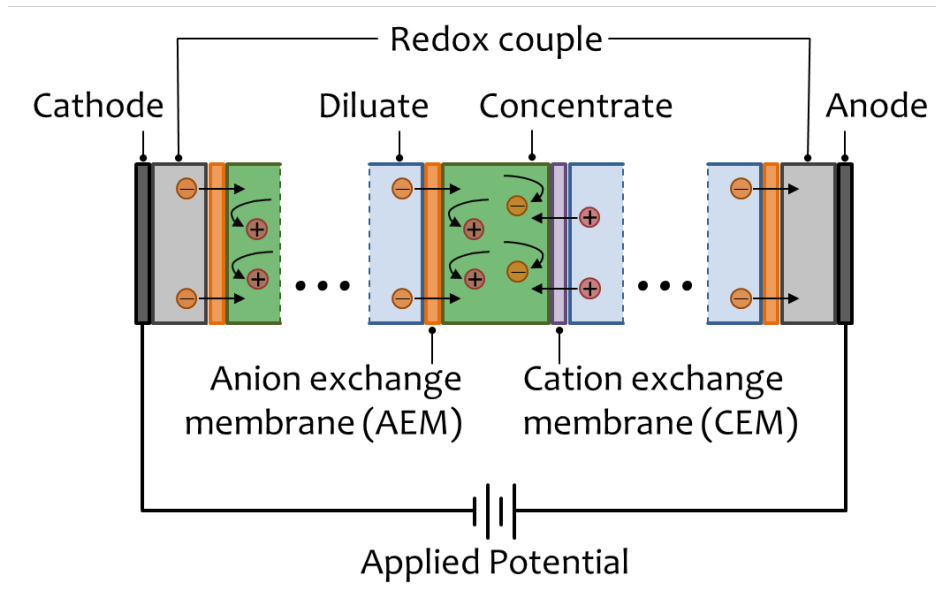


Figure 1-1. Schematic of ED, with the arrows indicating the direction of cation (+) and anion (-) permeation. Repeating pairs of CEMs and AEMs selectively allow the permeation of counterions while rejecting co-ions. Note that only one IEM pair and the end electrodes are shown. A reversible redox couple is circulated at the end electrodes to convert between the ionic current and the electric current.

ED affords several fundamental advantages. ED operates without water flux across the membrane, and the feed streams are not pressurized. Hence, fouling effects are significantly lower relative to another major desalination technology, reverse osmosis (RO), and, consequently, less pre-treatment of the feed stream is needed (Lindstrand et al. 2000, Strathmann 2004a, van der Hoek et al. 1998). Furthermore, the pressurizations of 50 bar (725 psi) and higher in typical seawater RO operation demands capital-intensive high-pressure pumps, pressure-exchange devices, and mechanically robust plumbing, whereas ED is not encumbered by such capital requirements (Younos 2005).

1.2 Project Needs

Although ED shows immense potential for desalination and ion separation applications, greater adoption of the technology is hindered by the chief limitations of relatively high-cost and inherently low-ionic conductivities of the IEMs. IEMs are polymeric thin-films of typically 50 to 200 μm with charged

functional groups attached to the polymer backbone, as depicted in Figure 1-2 (Baker 2012, Strathmann 2004a, Xu 2005b). The selectivity of IEMs is based on charge exclusion: the fixed charged groups exclude ions of the same charge (co-ions) from the membrane, while being permeable to oppositely charged ions (counterions) (Nagarale et al. 2006, Sata 2004, Strathmann 2010, Tanaka 2015, Xu 2005b). Thus, anion exchange membranes have fixed, positively charged groups that allow the permeation of anions, while cation exchange membranes have negatively charged groups to enable cation transport.

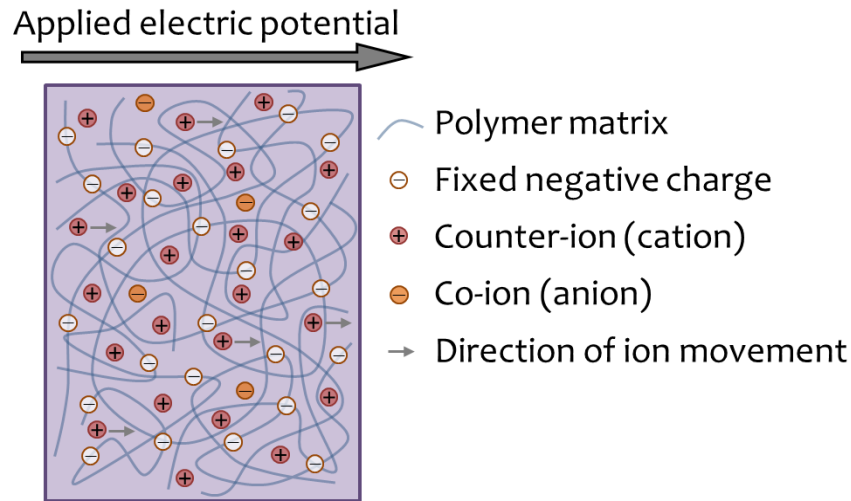


Figure 1-2. Schematic of a cation exchange membrane with fixed negative charges within the polymer matrix. Because of charge exclusion, co-ions (anions) are almost entirely excluded from the membrane matrix and, therefore, the CEM allows selective passage of counterions (cations), as indicated by the directional arrow.

A fundamental limitation of ED is the inherently low conductivity of conventional IEMs. The large contribution of the IEMs to the resistance of the ED stack results in high internal resistance in the ED circuit, consequently causing elevated ohmic losses that detrimentally lower the energy efficiency. However, an increase in conductivity (σ), the reciprocal of resistivity (i.e., $\sigma = 1/\rho$), is almost inevitably accompanied by a decrease in the permselectivity, α . Permselectivity is the ability of the membrane to transport only counterions (i.e., cations in CEMs or anions in AEMs) and exclude co-ions (i.e., anions in CEMs or cations in AEMs). A permselectivity of unity signifies perfect charge selectivity, whereas IEMs with $\alpha = 0$ do not discriminate between counter- and co-ions. A high permselectivity is imperative for effective desalination and ion separation. The negative slope of the green line in Figure 1-3 illustrates the conductivity-permselectivity trade-off relation of commercially available and laboratory-fabricated IEMs. To advance IEMs beyond their current high-resistance drawback without sacrificing ion selectivity, innovative membranes that break away from the conductivity-permselectivity trade-off are needed.

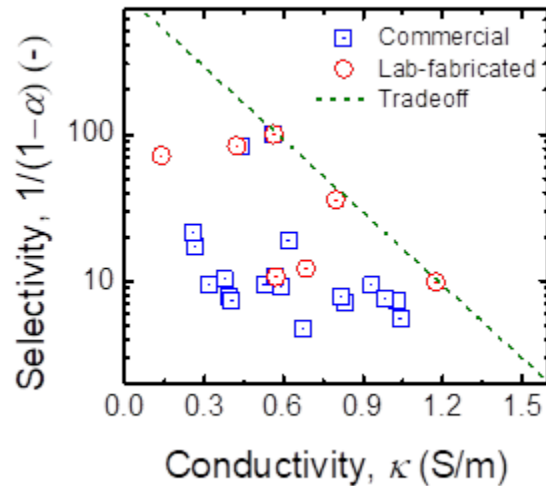


Figure 1-3. Selectivity of IEMs, presented as $1/(1-\alpha)$, as a function of conductivity, σ . The negative slope of the green line represents the empirical conductivity-permselectivity trade-off relation of IEMs, in which an increase in conductivity is accompanied by a decrease in permselectivity. Blue squares and red circles denote commercially available and laboratory-fabricated IEMs, respectively (Długołęcki et al. 2008a, Güler et al. 2013).

Nanocomposite IEMs with a percolating network of rationally functionalized, one-dimensional nanomaterials can attain high intrinsic conductivity while preserving permselectivity. Because of the large aspect ratio and the nanoscale dimensions, a given amount of non-aggregated one-dimensional nanomaterial, such as carbon nanotubes, can achieve several orders of magnitude greater dispersity than micro-scale fillers. When the filler content of composites exceeds a critical threshold value, termed the *percolation threshold*, a contiguous three-dimensional network of fillers is formed within the matrix.

Carbon nanotubes can be purposefully functionalized with specific moieties to confer desired properties to the nanomaterial. Rationally modified carbon nanotubes using functional groups, such as quaternary amines (+) and sulfonic acid (-), to achieve a high charge density can be dispersed in the polymer matrix during membrane fabrication to form a percolating network within the polymer thin-film. The continuous three-dimensional mesh of conductive carbon nanotubes can advantageously lower the intrinsic resistivity of the nanocomposite membrane while the charged functional moieties intensify the charge exclusion effect, thus sustaining a high permselectivity.

1.3 Project Objectives

The research aims to develop a nanocomposite IEM with better desalination performance. The aim involves the following five tasks:

Task 1. Analytical study on conductivity-permselectivity tradeoff

Fundamental understanding of the trade-off and its intrinsic relation to membrane properties is crucial to inform the development of better membranes. However, a complete fundamentals-based framework to describe the IEM conductivity-permselectivity relationship is lacking. Task 1 presents an IEM transport model to elucidate the dependence of key performance parameters, ionic conductivity and charge selectivity on intrinsic membrane chemical and structural properties. The transport models serve to guide the development of membranes with improved performance.

Task 2. Functionalization of carbon nanotubes

To enhance the stability of carbon nanotubes in casting solution and improve the dispersion in polymer matrix, carbon nanotubes are functionalized with desired chemical moieties. Tunable functionalization is important for further nanocomposite IEM development. To achieve this goal, two different pathways to sulfonated carbon nanotubes (sCNTs) were explored.

Task 3. Fabrication of nanocomposite ion-exchange membranes

The goal of Task 3 is to produce IEMs with a percolating network of carbon nanotubes. Sulfonated CNTs from the preceding task are used in the fabrication of the nanocomposite IEMs. A solvent evaporation method is employed for membrane fabrication.

Task 4. Characterization of fabricated nanocomposite IEM properties

The fabricated nanocomposite membranes are characterized to determine the structural, electrical, and transport properties. The investigated parameters of IEM include: ion-exchange capacity, swelling degree, membrane thickness (l), area-specific resistance (ASR) to ion transport, intrinsic conductivity (σ), and apparent permselectivity (α). The nanocomposite IEM characteristics are compared with pristine membrane controls (i.e., only consisting of ion-exchange polymers).

Task 5. Performance evaluation of fabricated nanocomposite IEMs in electro dialysis desalination

The fabricated and characterized membranes are tested in an electro dialysis set-up to evaluate the performance in brackish desalination. To assess the advantages of nanocomposite IEMs, the potential improvement on energy requirement for desalination is projected using stacked test results and common design dimensions.

2 Transport model for ion exchange membranes

In this chapter, a novel IEM transport model is presented to analytically relate conductivity and permselectivity to intrinsic membrane chemical and structural properties. The model employs the Nernst-Planck transport framework and incorporates counterion condensation theory to simulate the performance of IEMs in a range of ED operations. The analysis revealed the mechanism for the tradeoff induced by bulk solution concentration. The relationships between structural properties such as ion-exchange capacity, swelling degree, membrane thickness, and performance properties, such as conductivity and permselectivity, are also investigated using the simulation model. The results of modeling analysis offer systematic strategies to develop IEMs with improved conductivity and permselectivity.

2.1 Transport model development

For the transport model, the Nernst-Planck framework is adopted to describe the movement of ions driven by chemical and electrostatic potentials. Two assumptions commonly used for IEM studies are employed to derive boundary conditions: 1) electrochemical potential equilibrium at the solution-membrane interfaces, and 2) electroneutrality within the membrane matrix. The model incorporates counterion condensation theory to determine the activity coefficients and effective ion diffusivities within the membrane matrix. Computational codes numerically solve for the system of non-linear differential equations through a finite element method.

Output membrane performance parameters of the model include: current efficiency (CE), permselectivity (α), area specific resistance (ASR), area specific conductance (ASC), and conductivity (σ). Current efficiency is a measure of ionic current use in ED for separation and is similar to permselectivity at the process level. Conductance and conductivity are the reciprocals of resistance and resistivity, respectively.

Detailed information on the development of the transport model and description of the parameters are presented in the Appendix. In addition, the IEM transport model was validated using empirical data and showed good agreement (also detailed in the Appendix).

2.2 Influence of operating parameters

Here, the effects of operating parameters, applied voltage, and bulk solution concentrations on membrane performance are examined. Simulated membrane

properties of $c_{\text{fix}} = 1.68 \text{ eq/L}$, $f_w = 0.30$, $l = 100 \text{ }\mu\text{m}$, and $\xi = 1.08$ are held constant throughout this section.

2.2.1 Operating electric potential

CE and ASR as a function of ΔV^m for ED are shown in Figure 2-1. Concentration of the LC and HC solutions are 17 and $200 \times 10^{-3} \text{ mol/L NaCl}$, respectively, for ED to represent brackish water desalination to $1,000 \text{ ppm TDS}$ product water.

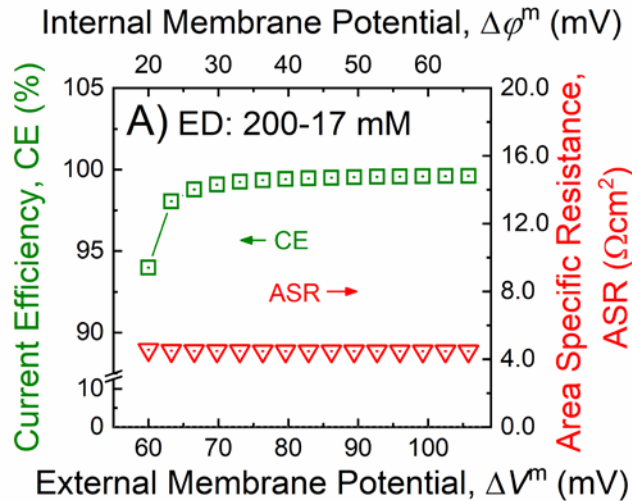


Figure 2-1. Current efficiency (CE; green square, left vertical axis) and area specific resistance (ASR; red triangles, right vertical axis) as a function of external electric potential difference across the membrane, ΔV^m for ED desalination of simulated brackish water at $200 \times 10^{-3} \text{ mol/L NaCl}$ to produce product water of $1,000 \text{ ppm TDS}$ ($= 17 \times 10^{-3} \text{ mol/L NaCl}$).

While ASR remains practically constant, current efficiency and, equivalently, permselectivity are dependent on ΔV^m , especially as $\Delta V^m \rightarrow$ open-circuit voltage (OCV = 58.5 mV). As higher voltage is applied in ED desalination, CE increases but eventually levels off (about 99.6 percent for the scenario simulated in Figure 2-1). This has been observed in a recent experimental study in which the counterion transport number increased and plateaued as applied voltage rose (Vardner et al. 2017). The dependence of CE and permselectivity on voltage has important implications for ED operation. Low operating voltage at around open-circuit voltage for electrodialysis should be avoided.

Membrane specifications provided by IEM manufacturers typically list the ASR and permselectivity or, more precisely, the apparent permselectivity ($\alpha_{\text{app}} = \text{OCV}$ divided by Nernst potential); such practice is also common in IEM studies (Geise et al. 2013, Guler et al. 2013, Guler et al. 2012). However, both ASR and apparent permselectivity are not intrinsic membrane properties but, rather, are dependent on the operating conditions. This analysis and previous studies indicate ASR is

effectively constant across the typical voltage range, but variation in permselectivity is significant and non-negligible. Hence, substantial error may be incurred if apparent permselectivity is used to approximate actual α during operation, because typical ED uses ΔV^m significantly far away from the open-circuit voltage. For the rest of the simulations in this study, ΔV^m is set at 200 percent open-circuit voltage for ED to enable consistency in comparison.

2.2.2 External solution concentrations

CE and ASC are investigated for a range of bulk solution concentrations. Figure 2-2 shows CE and ASC as a function of concentrate channel concentration ($c^{s,HC}$, 0.1 to 1.2 mol/L NaCl), simulating the desalination process with brackish water to hypersaline water (Yip et al. 2016).

The CE is negatively related to bulk concentration. In brackish water ED desalination, in which the input feed stream is significantly lower than 35,000 ppm TDS (about 0.6 mol/L NaCl), the external solution concentrations are not sufficiently high to detrimentally affect co-ion exclusion (e.g., CE = 99.8 percent for $100\text{--}50 \times 10^{-3}$ mol/L NaCl). Presently available IEMs, however, are not suitable for desalination of seawater or hypersaline feeds because of ineffectual selectivity. Higher salinity seriously weakens co-ion exclusion and causes poor current efficiencies (e.g., 84.7 percent for the simulated membrane in 1.2-0.6 mol/L NaCl, representing desalination of seawater to brine twice as saline).

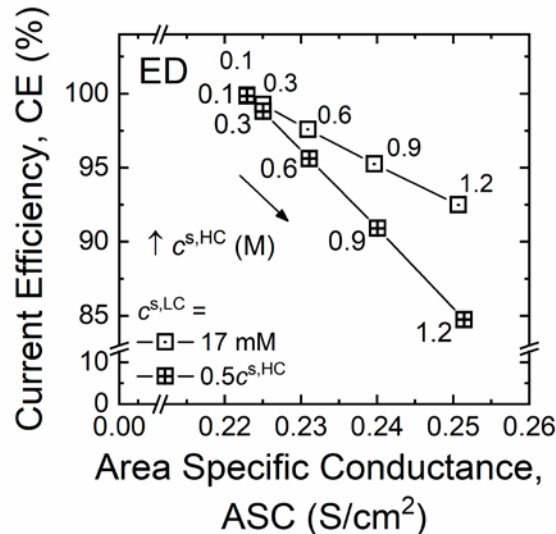


Figure 2-2. CE and ASC (vertical and horizontal axes, respectively) with $c^{s,HC}$ increasing from 0.1 to 1.2 mol/L NaCl in ED (data point labels), representing desalination of brackish water to brine twice the concentration of seawater.

Whereas permselectivity is adversely affected by higher bulk concentration, membrane conductance is favorably raised, although the improvement is modest. For $c^{s,LC} = 17 \times 10^{-3}$ mol/L NaCl, ASC increases from 0.223 to 0.250 S/cm^2 for

the simulated IEM by raising $c^{s,HC}$ from 0.1 to 1.2 mol/L NaCl (Figure 2-2). The marginal conductivity improvement is due to the greater ion concentration within the membrane matrix when bulk concentration is high. The increased ionic current is carried by both counter- and co-ions, thereby accounting for the concomitant compromise in permselectivity. With greater LC solution concentrations, enhancements in membrane ionic conductivity are more pronounced, but still relatively small.

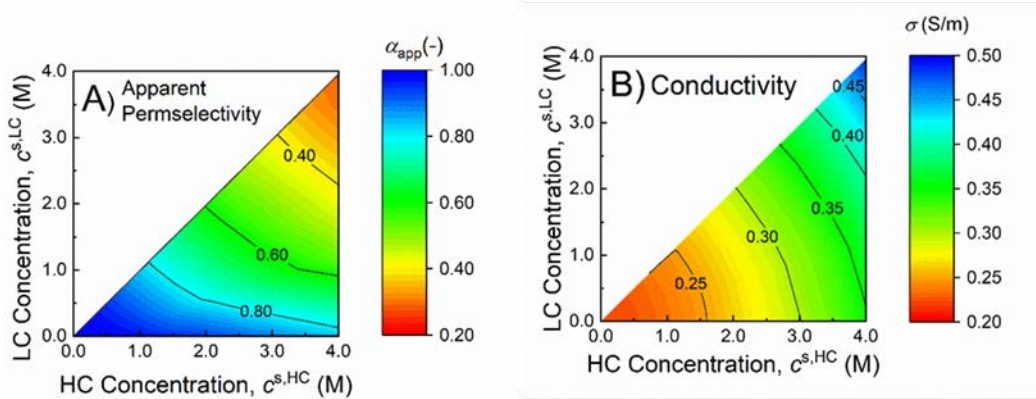


Figure 2-3. Contour plot of A) apparent permselectivity and B) conductivity as functions of HC and LC bulk solution NaCl concentrations (horizontal and vertical axes, respectively).

Thus, the operating condition of external solution concentrations produces a trade-off between conductivity and current efficiency, as represented by the negative slopes of the ASC-CE trendlines in Figure 2-2, where increasing the bulk concentrations undesirably depresses membrane selectivity for counterions but slightly benefits conductivity. The trade-off trend was seen consistently in simulations with membranes of different properties that are typical for current commercially available IEMs. This trade-off has also been observed in recent experimental studies (Galama et al. 2014, Geise et al. 2014a, Kamcev et al. 2018). The concentration dependence of membrane conductivity was explained within the Nernst-Einstein framework for IEM in an iso-concentration environment (i.e., $c^{s,HC} = c^{s,LC}$ and $d\mu_i/dx = 0$) (Kamcev et al. 2018). The transport model in this study further extends the theoretical rationale to encompass the more general scenario in which there is a chemical potential gradient across the membrane that is representative of ED and reverse electrodialysis (RED) operation.

The model presented here can be a useful tool to quantitatively approximate the trade-off between permselectivity, α , and conductivity, σ , at varying external concentrations. Simulated apparent permselectivity, α_{app} , and σ for different HC and LC solution concentrations are summarized in Figure 2-3 for the representative IEM analyzed thus far ($c_{fix} = 1.68$ eq/L, $f_w = 0.30$, and $l = 100$ μm). Apparent permselectivity is commonly adopted for experimental characterization of IEMs (Sata 2007, Strathmann 2004b) and is reported here to avoid the

discrepancy arising from different applied voltages and operating modes. Conductivity for ED is averaged across current density of -20 to 20 mA/cm². The permselectivity data of Figure 2-3 are in very good agreement with reported empirical results (Daniilidis et al. 2014). Limitations to the operating regime of ED are clearly displayed: employing IEMs in salinities beyond seawater concentration significantly diminishes the permselectivity with only a marginal gain in conductivity, thus confining ED to brackish water desalination.

2.3 Influence of structural properties

Because ion-exchange capacity, swelling degree, thickness, fixed charge density, and water volume fraction of IEMs are intricately linked (Geise et al. 2014b, Xu 2005a), experimental approaches to investigate the impact of a single parameter on ED are inevitably confounded by other properties that are simultaneously altered. On the other hand, the analytical framework employed in this study enables the influence of individual intrinsic membrane properties to be isolated for systematic examination. As such, the approach can more clearly elucidate the significance of the role played by the parameter and inform rational customization of IEM properties for improved overall performance. Throughout this section, except for the parameter being inspected, all other IEM properties are held constant at ion-exchange capacity = 2.0 meq/g, swelling degree = 0.36 , $l = 100$ μm , $\xi = 1.08$, and polymer density, $\rho_p = 1.2$ g/mL. The range of membrane structural properties investigated here are representative of common values reported in literature (Hong et al. 2015, Kamcev et al. 2017b, Ran et al. 2017). Unless stated otherwise, $c^{\text{s,HC}} = 200 \times 10^{-3}$ mol/L NaCl and $c^{\text{s,LC}} = 100 \times 10^{-3}$ mol/L NaCl to simulate brackish water ED desalination.

2.3.1 Ion exchange capacity

Ion-exchange capacity is the number of fixed charges per unit weight of dry polymer (Strathmann 2004b). The ion-exchange capacity of typical commercial IEMs is in the range of 1 to 3 meq/g (Xu 2005a). Fixed charge density (c_{fix}), charges normalized by the total volume of water-swollen membrane, describes the density of charged moieties in wet state. c_{fix} and ion-exchange capacity are related by the degree of hydration (which is characterized by the water volume fraction): $c_{\text{fix}} = (1-f_w)$ ion-exchange capacity. Figure 2-4 shows the equilibrium counter- and co-ion concentration ratio within the membrane as a function of external solution concentration, for different fixed charge densities. The ratio of counter- to co-ions in membrane ($c_{\text{ct}}^m/c_{\text{co}}^m$) is related to fixed charge density by an approximately second-order power law for bulk concentration $c^{\text{s}} \ll c_{\text{fix}}$: as c_{fix} increases six-fold from 0.5 to 3.0 eq/L, $c_{\text{ct}}^m/c_{\text{co}}^m$ rises approximately 36 times (i.e., $c_{\text{ct}}^m/c_{\text{co}}^m \propto c_{\text{fix}}^2$). Thus, an IEM with higher c_{fix} can uphold a certain $c_{\text{ct}}^m/c_{\text{co}}^m$ in a more concentrated

bulk solution (i.e., maintain reasonable co-ion exclusion). Additionally, the counterion concentration is approximately equal to the fixed charge density to achieve charge balance. Hence, c_{fix}^m is critical for determining c_{ct}^m and c_{co}^m within the IEM.

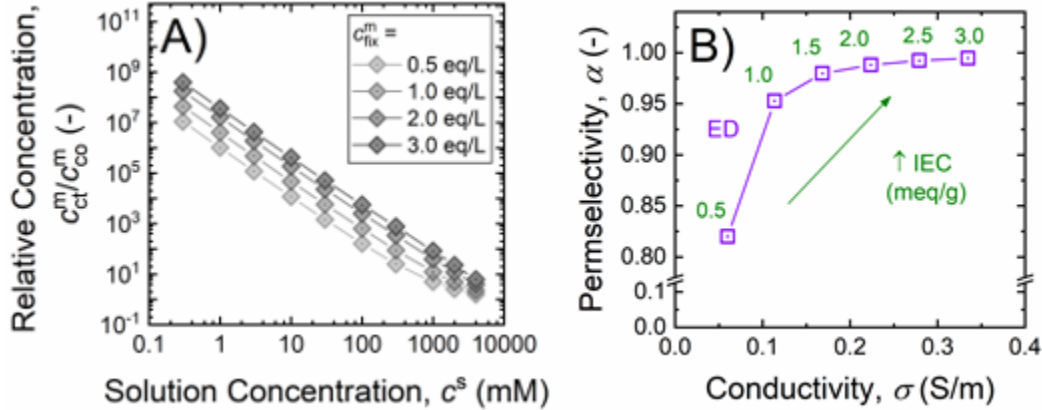


Figure 2-4. A) Relative concentration of counter- to co-ions, as a function of bulk solution concentration for different membrane fixed charge densities. Note that both axes are on logarithmic scale. B) Permselectivity, α , and conductivity, σ , with increasing membrane ion-exchange capacity for ED.

The impact of ion-exchange capacity on conductivity and permselectivity is depicted in Figure 2-4B. Raising ion-exchange capacity from 1.0 to 3.0 meq/g enhances α from 0.953 to 0.995 and σ increases from 0.113 to 0.335 S/m (i.e., increasing the ion-exchange capacity is simultaneously beneficial for conductivity and permselectivity). This trend is corroborated by experimental studies, as summarized in recent review articles (Hong et al. 2015, Ran et al. 2017).

The influence of ion-exchange capacity on α and σ can be intuitively understood in the framework of chemical potential equilibrium and transport governed by the Nernst-Planck equation. With higher fixed charge density, exclusion of like-charged co-ions is enhanced (Figure 2-4A), which is beneficial to the selective transport of counterions over co-ions. At the same time, to preserve electroneutrality, an increase in the density of fixed charged groups raises the counterion concentration within the membrane matrix. Having more current carriers of mobile ions within the IEM yields greater ion fluxes that lead to better conductivity. Hence, increasing ion-exchange capacity is a direct method to simultaneously improve the key IEM performance parameters of permselectivity and ionic conductivity.

However, the approach of increasing ion-exchange capacity to attain more conductive and selective membranes is chemically and physically constrained in practice. Conventional IEMs have charged functional groups on the polymer matrix. Therefore, the functionalization chemistry imposes an upper limit on the achievable ion-exchange capacity. Additionally, when the concentration of fixed

charge groups approaches within an order of magnitude of the ionization constant (i.e., K_a or K_b), a significant fraction of the moieties will be unionized (Takamuku et al. 2015), effectively lowering c_{fix} . Finally, intensifying ion-exchange capacity increases the polymer hydrophilicity that consequently raises the swelling degree of the IEM (Cho et al. 2017, Cui et al. 1998). Membrane swelling due to water hydration dilutes c_{fix} and thus opposes the α and σ benefits of the enhanced ion-exchange capacity. Furthermore, greater water sorption exerts mounting osmotic swelling pressure on the polymer network. Beyond a certain point, the expansion stress exceeds the mechanical stability of the membrane and the polymer matrix ceases to form the required thin film (He et al. 2015, Kariduraganavar et al. 2006). These restrictions curtail the practically attainable fixed charge density for conventional IEMs.

2.3.2 Swelling degree

Swelling degree, defined as the volume of water in the swollen IEM per unit polymer mass (i.e., dry membrane weight) (Strathmann 2004b), indicates the extent of membrane hydration. The volume fraction of water in the IEM, f_w , is related to swelling degree by:

$$f_w = \frac{\text{SD}}{\text{SD} + \rho_p^{-1}}$$

where ρ_p is the density of dry polymer. The water volume fraction, in turn, affects tortuosity, τ , which describes the lengthened diffusional pathway across the water-swollen membrane, and can be approximated by considering that ion transport is excluded from the stationary polymer chains (Mackie and Meares 1955a, b):

$$\tau = \frac{(2 - f_w)^2}{f_w}$$

The effective ion diffusivity ratio in water-swollen polymer to bulk aqueous phase is $D^m/D^s = f_w/\tau$. Swelling reduces the tortuosity of ion-exchange polymer, which raises the ion mobility inside membrane.

Figure 2-5 depicts f_w , τ , and c_{fix} as a function of swelling degree over the typical range for current IEMs (Guler et al. 2013). As denoted by the above equations, a larger swelling degree augments the water volume fraction of the membrane matrix and reduces the tortuosity (blue triangle and violet diamond symbols, primary and secondary left vertical axes, respectively). For a given ion-exchange capacity (fixed at 2.0 meq/g in this simulation), c_{fix} is inversely proportional to swelling degree: altering the swelling degree to higher levels dilutes c_{fix} (green pentagon symbols, right vertical axis). As discussed earlier, the c_{fix} decline is

unfavorable because the equilibrium c_{ct}^m is lowered, which negatively influences conductivity. As such, increasing the IEM swelling degree is expected to produce opposing effects of reduced conductivity due to lowered fixed charge density, and enhanced ion transport because of increased water volume fraction and decreased diffusional path length.

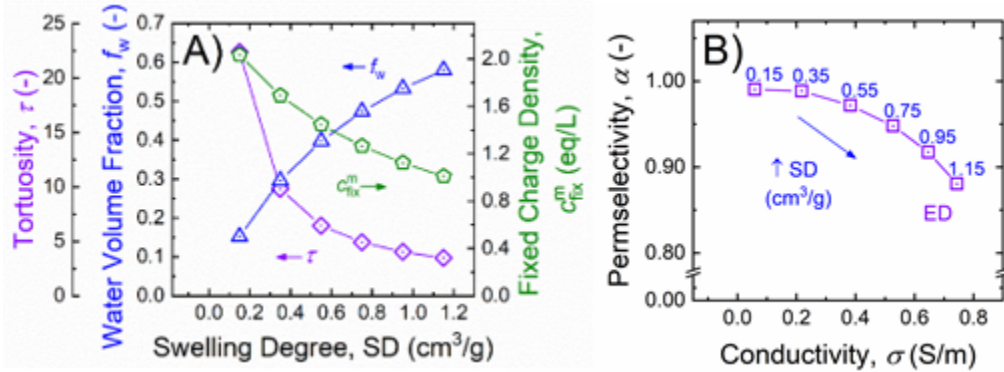


Figure 2-5. A) Water volume fraction, f_w , membrane tortuosity, τ (primary and secondary left vertical axes: blue triangle and violet diamond symbols, respectively), and fixed charge density, c_{fix}^m (right vertical axis, green pentagon symbols), as a function of swelling degree. B) Permselectivity, α , and conductivity, σ , with increasing swelling degree.

Varying swelling degree while keeping ion-exchange capacity and other membrane parameters constant produces a trade-off between conductivity and permselectivity, as presented in Figure 2-5B. When swelling degree is raised from 0.15 to 1.15 cm^3/g in the simulations, conductivity in ED increases from 0.059 to 0.744 S/m, while permselectivity drops from 0.997 to 0.813. This trade-off trend is reproducible across the range of typical membrane properties (results not shown) and is in agreement with reported observations of experimental studies (Długołęcki et al. 2008b, Geise et al. 2013, Guler et al. 2013).

The effect of swelling degree on σ and α can be explained with the IEM transport model presented in this study. As discussed earlier, when swelling degree increases, membrane tortuosity drops and water volume fraction is augmented (Figure 2-5A), consequently boosting the effective ion diffusivities. According to the Nernst-Planck equation, an increase in the diffusivity yields a proportional gain in ion flux that leads to enhanced conductivity. Although the lower c_{fix} due to a higher swelling degree has negative impact on conductivity (because of reduced ion concentration within the membrane matrix; see earlier discussion), the benefits to IEM structure outweigh the drawback, and net σ enhancement is attained. This trend of increased σ with greater swelling degree has been reported in a previous study, in which a four-fold increase in intrinsic conductivity was achieved when swelling degree was raised from 0.167 to 0.295 cm^3/g . (Cui et al. 1998). This empirical result matches with the simulation presented in Figure 2-

5B: raising swelling degree from 0.15 to 0.35 cm³/g improved σ about 3.7 times. Further, the analysis indicates that a more than tenfold enhancement in conductivity can be attained by increasing membrane swelling degree from 0.15 to 1.15 cm³/g.

The detrimental effect of greater swelling degree on permselectivity can be rationalized by the dilution of c_{fix} (Figure 2-5). A reduction in c_{fix} weakens the charge exclusion effect of the IEM, leading to a compromised α . Empirical results of a recent study demonstrated that the permselectivity decreased when swelling degree was lowered for the same ion-exchange capacity (Cho et al. 2017), corroborating the findings of this analysis.

Thus, membrane swelling degree has strong bearing on the key performance parameters of σ and α . Factors such as polymer structure, configuration, and crosslinking degree influence swelling degree (Geise et al. 2014b, Toomey et al. 2004) and, hence, can be design levers to tune the balance between conductivity and permselectivity for customized IEM performance. Additionally, a higher swelling degree would likely lead to a correspondingly larger membrane wet thickness that would yield a lower ASC, or equivalently, greater ASR. The analysis presented in Figure 2-5 excludes the effect of l by using thickness-normalized conductivity, σ . The influence of IEM thickness is examined in the next section.

2.3.3 Membrane thickness

The effects of IEM thickness, l , on permselectivity and ASC ($= \sigma/l$) are shown in Figure 2-6. Because ASC and the reciprocal ASR are area-specific (i.e., membrane thickness effects are incorporated), they are of practical relevance in stack design for ED processes. Assuming fixed ion-exchange capacity and swelling degree (ion-exchange capacity = 2.0 meq/g and $f_w = 0.30$) yields a constant conductivity that is independent of l . As the length of transport pathway scales with IEM thickness, ASR increases proportionally with membrane thickness. Conversely, ASC declines inversely from 0.373 to 0.112 S/cm² when l increases from 60 to 200 μm (crossed symbol, right vertical axis of Figure 2-6). The trends of thickness-independent conductivity and $\text{ASR} \propto l$ are supported by empirical results of previous experimental studies (Hwang et al. 1999, Wang et al. 2009). Hence, thinner membranes advantageously enhance ASC for IEM applications.

Crucially, the analysis shows that permselectivity is independent of membrane thickness. For the simulated l range that is representative of current commercial IEMs (Sata 2007, Xu 2005a), α is not effectively changed (0.988). The trend of preserved α with decreasing thickness is valid for the constant ΔV^{m} applied in this analysis. However, operating thinner IEMs under constant current can result in

lowered permselectivity due to ΔV^m approaching the open-circuit voltage with the improved conductivity (refer to the discussion in Section 2.2.1), and as reported in a recent experimental study (Tedesco et al. 2018). Reducing membrane thickness can produce lower resistance while preserving permselectivity to improve the overall performance of IEM-based technologies. However, the technical limitations inherent to current IEM fabrication techniques (e.g., solvent evaporation casting, polymer blending and pore filling (Ran et al. 2017)), together with the need for adequate mechanical robustness and defect-free films, will constrain how thin the membranes can get. Hence, improvements in manufacturing methods and development of stronger materials are potential routes to robust ultrathin IEMs.

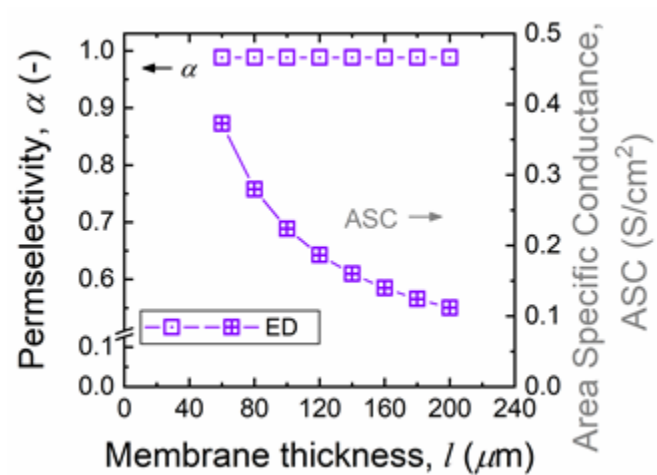


Figure 2-6. Permselectivity (α ; dotted symbols, left vertical axis) and ASC (crossed symbols, right vertical axis) as a function of membrane thickness, l .

2.4 Implications

This study presents an IEM transport model that employs counterion condensation theory to analytically determine the experimentally inaccessible parameters of ion activity and diffusivity, and overcome a critical limitation hindering the application of the Nernst-Planck framework within the membrane matrix. The approach uses only intrinsic membrane properties (i.e., without additional fitting parameters) to determine process performance parameters that are in good agreement with reported measurements of experimental studies. While ionic conductivity, or equivalently, resistance and permselectivity, are commonly reported by membrane manufacturers and in literature as “IEM properties,” this analysis shows that σ and α are process-specific parameters that depend on operating conditions of applied voltage and bulk solution concentration and are not truly inherent to the membrane. Instead, intrinsic membrane chemical and structural properties, such as ion-exchange capacity and swelling degree, are more useful process-independent parameters for benchmarking IEM performance.

The conductivity-permselectivity trade-off observed in recent experimental studies is reproduced with the simulations here, and the fundamental mechanisms governing the interwoven relationship are laid out in the context of the Nernst-Planck framework: increasing the bulk solution concentration suppresses the charge-exclusion ability of the IEM, thereby reducing permselectivity but enhancing conductivity due to greater ion concentration within the membrane matrix. Raising the swelling degree amplifies the effective ion diffusivity and improves conductivity, but concomitantly compromises permselectivity because the fixed charge density is diluted. The analysis identifies the theoretical basis for the confined application of IEMs to sub-seawater salinities. Therefore, as is presently practiced, ED is only suitable for brackish water desalination. There has been recent interest in using hypersaline streams of saltworks brine and seawater desalination concentrate for reverse ED power generation (Tedesco et al. 2015a, Tedesco et al. 2017, Tedesco et al. 2015b, Tedesco et al. 2016).

Performance of IEMs has advanced steadily over the years (Hong et al. 2015, Ran et al. 2017, Xu 2005a) and the structure-property analysis of IEM transport presented here can further inform the rational development of customized membranes. Increasing the ion-exchange capacity should simultaneously enhance conductivity and permselectivity, but would also be accompanied by greater IEM swelling as the more densely charged film exhibits greater hydrophilicity and sorbs more water from the bulk solutions. The elevated membrane swelling further improves conductivity but is at the expense of a lower permselectivity, as governed by the trade-off relationship. Innovating fabrication techniques to drive the film thickness down while still maintaining adequate mechanical robustness offers the prospect of substantial gains in ionic conductivity without sacrificing permselectivity. The results also reveal the significance of developing novel methodologies (like nanocomposite IEMs), beyond altering those conventional structural properties, such as ion-exchange capacity and swelling degree. The model deepens the understanding of the intrinsic relationships behind the conductivity-permselectivity trade-off, which offers important guidance for the development of nanocomposite IEMs.

3 Carbon nanotubes functionalization and characterization

3.1 Materials and Methods

3.1.1 Materials

The pristine multiwall carbon nanotubes (diameter 20 to 30 nm, length 10 to 30 μm , purity 95 percent) were purchased from Cheap Tubes Inc. (USA) and used as

received. Concentrated sulfuric acid (H₂SO₄, 98%, Fisher Scientific), acetic anhydride (Fisher Scientific), methanol (Fisher Scientific), concentrated nitric acid (HNO₃, 70%, Fisher Scientific), thionyl chloride (SOCl₂, Sigma-Aldrich), dimethylformamide (Fisher Scientific), tetrahydrofuran (THF, Fisher Scientific), aminomethanesulfonic acid (Fisher Scientific), sodium hydroxide (Fisher Scientific), triethylamine (TEA, Sigma-Aldrich), indium foil (Fisher Scientific), poly(2,6-dimethyl-1,4-phenylene oxide) (PPO, Sigma-Aldrich), chloroform (Fisher Scientific), chlorosulfonic acid (Sigma-Aldrich), dimethyl sulfoxide (DMSO, Fisher Scientific) and sodium chloride (Fisher Scientific) are reagent grade and used as received. Water was purified with a Milli-Q system (Millipore Co.). PTFE filter membrane (0.2 μm pore size, diameter 47 mm) was purchased from Fisher Scientific and used as received.

3.1.2 Synthesis of sulfonated CNT

Two methods are employed to synthesize sulfonated CNT (sCNT): the acetyl sulfuric acid method and the acyl chloride method.

Method 1: acetyl sulfuric acid method

Method 1 consists of the following steps:

1. Place 40 mL acetic anhydride into a 100 mL round-bottom flask.
2. Slowly add 20 mL concentrated sulfuric acid to the flask with acetic anhydride.
3. Place the flask in an ice-water bath and stir vigorously for 30 minutes.
4. Add 40 mg pristine CNT (pCNT) to the mixture and sonicate for 30 minutes in an ice-water bath.
5. Stir the mixture at 80° C for 24 hours.
6. Dilute the resulting product with 200 mL ultrapure water.
7. Vacuum-filtered the resulting product with a PTFE membrane and wash with ultrapure water and methanol three times each.
8. The sulfonated CNT (sCNT) is dried in a vacuum oven at 80° C for 12 hours.

This process is illustrated in Figure 3-1 (Wei et al. 2015) and the experimental procedures are shown in Figure 3-2.

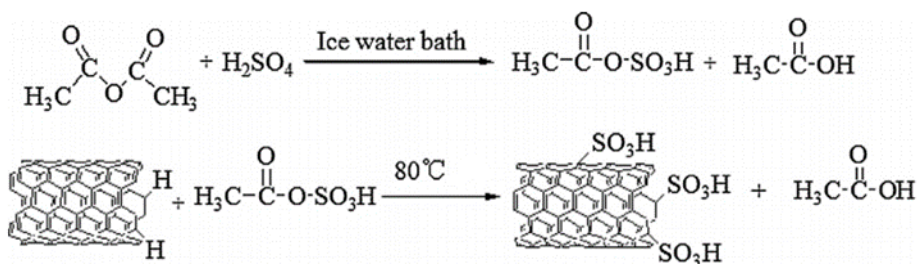


Figure 3-1. Schematic of the acetyl sulfuric acid method (Wei et al. 2015).

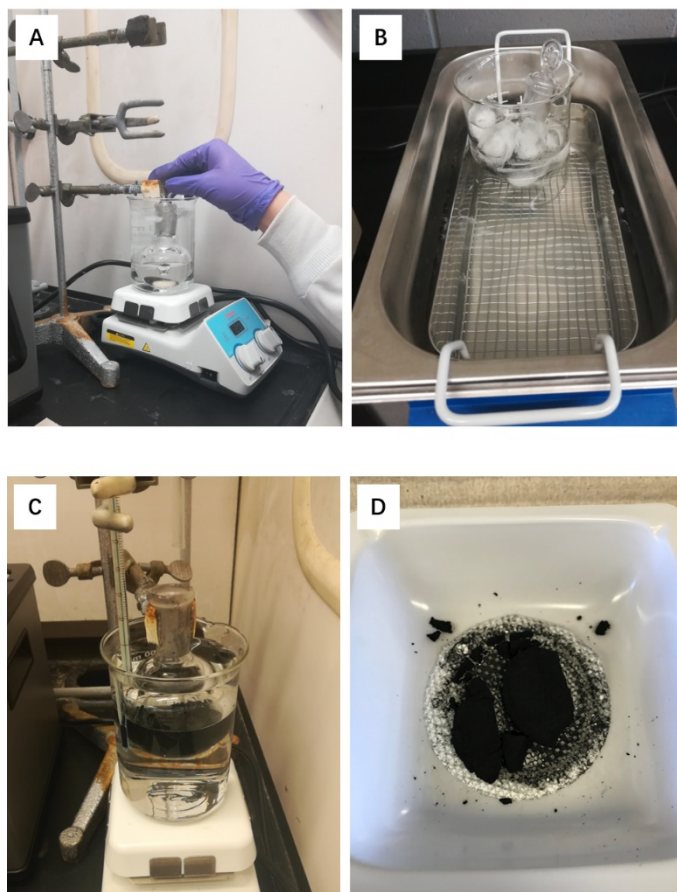


Figure 3-2. Experimental procedures of the acetyl sulfuric acid method: A) Concentrated sulfuric acid and acetic anhydride are stirred in an ice-water bath to generate acetyl sulfuric acid; **B)** pCNT is dispersed in the acid mixture by sonication in an ice-water bath (the ice-water bath prevents acetyl sulfuric acid from being converted to sulfoacetic acid (Moulder et al.), which is undesirable for subsequent reactions); **C)** the mixture was stirred at 80°C to allow acetyl sulfuric acid to react with C-H defects on pCNT; **D)** product sCNT.

Method 2: acyl chloride method

Method 1 consists of the following steps:

1. Place 200 mg pCNT in a 100 mL round-bottom flask with 40 mL acid mixture of concentrated H_2SO_4 and concentrated HNO_3 (3:1 by v%).
2. Sonicate the mixture for 30 min and then stir the mixture at 50° C under reflux for 2 hours. This step of acid treatment oxidizes pCNT and creates carboxylic groups on the CNTs (Jiang et al. 2005, Wang et al. 2005).
3. Dilute the resulting suspension with 200 mL ultrapure water, then vacuum-filter the mixture with a PTFE membrane and wash it with ultrapure water five times.
4. Dry the oxidized pCNT (CNT-COOH) in a vacuum oven at 60° C for 12 hours.

5. After the acid treatment, add CNT-COOH powder to a 100 mL round-bottom flask containing 40 mL SOCl₂ and 2 mL dimethylformamide.
6. Sonicate the mixture in an ice-water bath for 1 hour and stir it under reflux at 70° C for 24 hours.
7. Vacuum-filter the resulting mixture with a PTFE membrane, wash the mixture with THF three times, then dry it in a vacuum oven at 60° C for 1 hour. This step converts the carboxylic groups to acyl groups in CNT (CNT-COOH to CNT-COCl) (Gromov et al. 2005, Hamon et al. 1999).
8. Place 2 g aminomethanesulfonic acid, 1.6 g sodium hydroxide, obtained CNT-COCl powder, and 60 mL ultrapure water in a 100 mL round-bottom flask.
9. Sonicate the mixture for 30 minutes and stir it under reflux at 80° C for 24 hours.
10. Vacuum-filter the resulting suspension with a PTFE membrane, wash it with ultrapure water and methanol three times each, then dry it in a vacuum oven at 80° C for 12 hours. In the third step, aminomethanesulfonic acid reacts with the CNTs through the amidation reaction between acyl chloride group of CNT-COCl and amine group of aminomethanesulfonic acid (Yun et al. 2011). This method is illustrated in Figure 3-3 (Yun et al. 2011) and corresponding experimental procedures are shown in Figure 3-4.

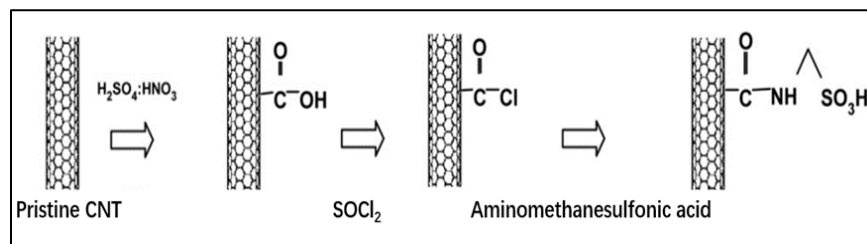


Figure 3-3. Schematic the acyl chloride sulfonation method (Yun et al. 2011).

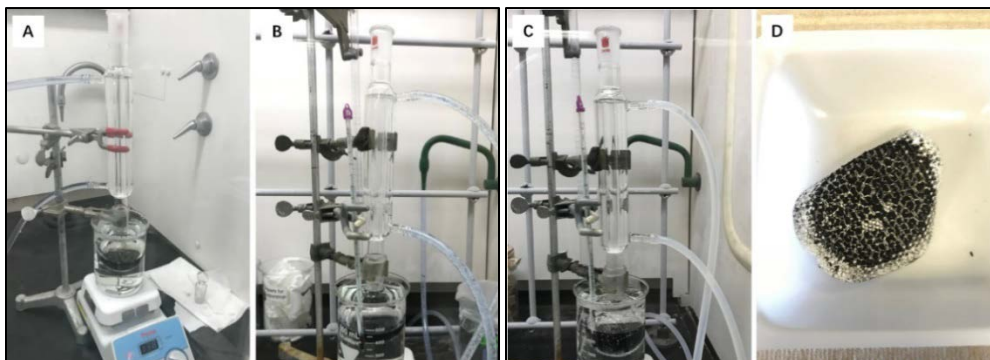


Figure 3-4. Experimental procedures of the acyl chloride sulfonation method: A) pCNT is stirred under reflux in H₂SO₄ and HNO₃ (3:1 by v%) at 80° C; B) CNT-COOH is stirred under reflux in SOCl₂ at 70° C; C) CNT-COCl is stirred under reflux in aminomethanesulfonic acid solution with addition of sodium hydroxide at 80° C; D) product sCNT.

3.1.3 Preparation of sulfonated CNT for characterization

X-ray photoelectron spectroscopy (XPS) analysis is conducted with Phi 5500 XPS (USA). Mg was used as the X-ray source with a work function of 4.5 eV.

AugerScan was used for data collection, curve fitting, and quantitative analysis. sCNT powder was pressed onto the surface of an indium foil substrate (Figure 3-5).



Figure 3-5. sCNT powder on indium foil substrate for XPS analysis.

3.2 Characteristics of functionalization CNT

3.2.1 Stabilized sulfonation result of Method 1

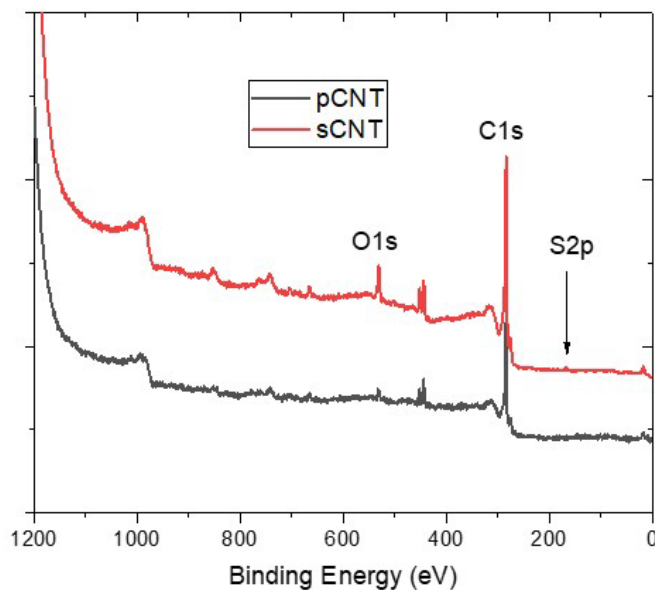


Figure 3-6. Full XPS spectrum of pCNT (gray) and sCNT using method 1 (red).

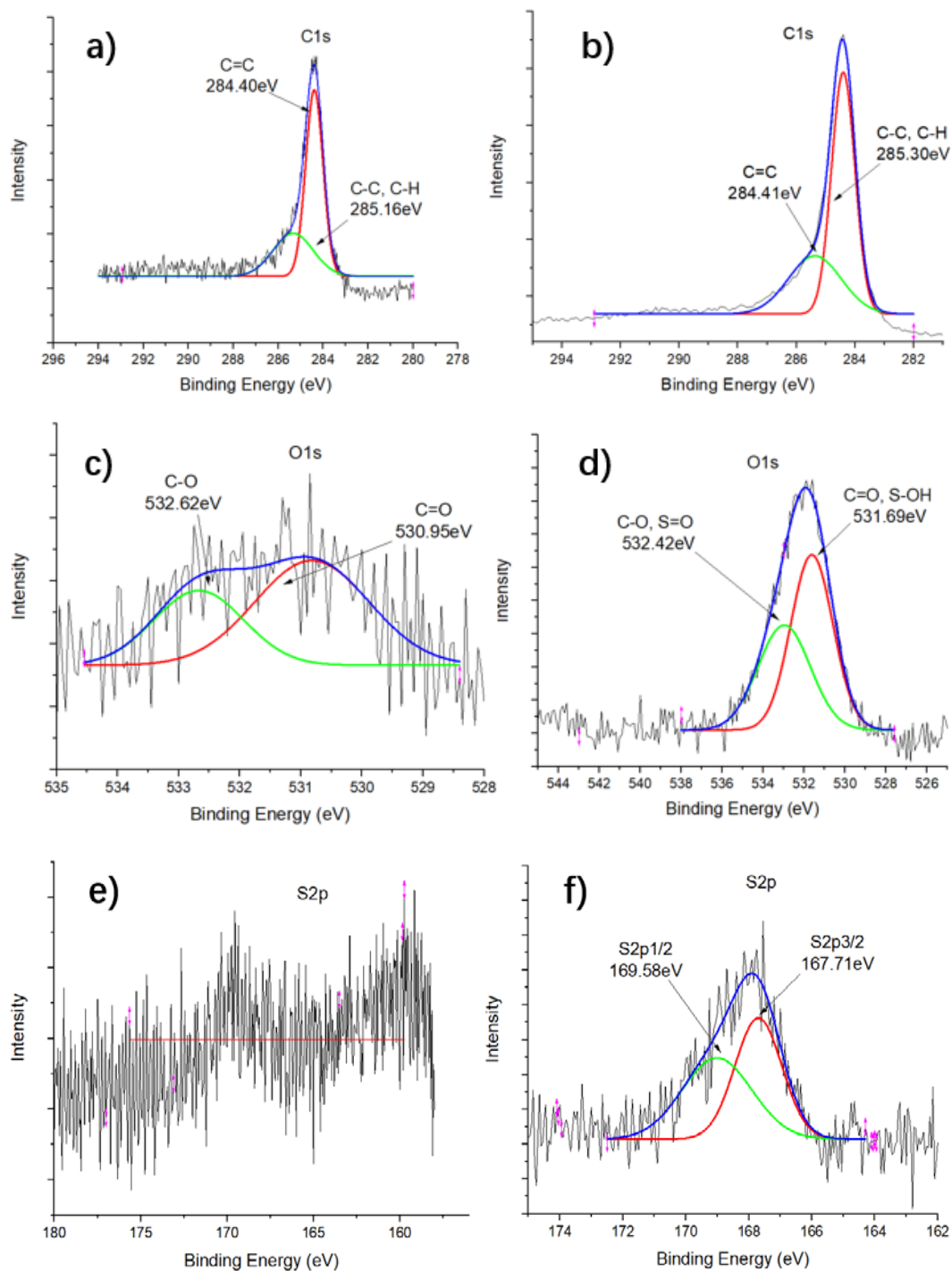


Figure 3-7. XPS detailed spectra of pCNT (left column): a) C1s spectrum, c) O1s spectrum, e) S2p spectrum; sCNT using method 1 (right column): b) C1s spectrum, d) O1s spectrum, f) S2p spectrum.

The XPS survey spectra of pCNT and sCNT sulfonated by method 1 are presented in Figure 3-6 and Figure 3-7, showing the elemental composition of the material. The full spectrum of pCNT shows a sharp carbon peak and a weak peak

at oxygen in Figure 3-6, in which the oxygen peak is due to defects on pCNT. For sCNT, the XPS full spectrum demonstrates a small sulfur peak in addition to two large peaks of carbon and oxygen. The two relatively weak peaks at around 450 eV are the signal of the indium substrate. In the detailed spectra of pCNT, the carbon peak can be decomposed into C=C (284.40 eV) and C-C and C-H (285.16 eV) (Figure 3-7a), and the oxygen peak is decomposed into C=O (530.95 eV) and C-O (532.62 eV) (Figure 3-7c). No peak could be identified at the binding energy of sulfur (Figure 3-7e), indicating that sulfur is not present in pCNT. As for the case of sCNT, the carbon peak can be mainly decomposed into C=C (284.41 eV) and C-C and C-H (285.30 eV) (Figure 3-7b), and the oxygen peak is decomposed into C=O and S-O (531.69 eV) and C-O and S=O (532.42 eV) (Figure 3-7d), suggesting that the nanotubes are still intact since the carbon and oxygen spectra are very close to that of pCNT. Most importantly, a sulfur peak is observed in the S2p spectrum and can be decomposed into S2p1/2 at 169.58 eV and S2p3/2 at 167.71 eV (Figure 3-7f), which indicates the existence of a sulfate group in sCNT. These results match the XPS characteristics of CNT sulfonation reported in literature (Wei et al. 2015).

By using the relative sensitivity factors of each element (0.296 for C, 0.711 for O and 0.666 for S) (Moulder et al.), the quantitative result of both pCNT and sCNT can be calculated and is summarized in Table 3-1. The concentration of sulfur in sCNT is around 3.5 w/w%, and no sulfur was detected in the pCNT. The sCNT fabricated by this method has an equivalent $-\text{SO}_3\text{H}$ ion-exchange capacity of around 1.1 meq/g and is comparable to the ion-exchange capacity of sulfonated polymer for membrane fabrication (approximately 1.0-1.6 meq/g). This result satisfied our expectation, and CNT sulfonated by this method was used in the fabrication of nanocomposite ion-exchange membrane.

Table 3-1. Atomic composition of pCNT and sCNT using method 1.

Sample	Peak area			Atom ratio (C : O : S)	Weight percentage (C% : O% : S%)	Ion-exchange capacity of $-\text{SO}_3\text{H}$ (meq/g)
	C	O	S			
pCNT	13997	2557	-	1:0.076:0	90.8:9.8:0	-
sCNT	12768	4186	471	1:0.136:0.016	81.7:14.8:3.5	1.1

3.2.2 Dispersion of sCNT in polar solvents

The dispersion of pCNT and sCNT in polar solvents was investigated by adding 5 mg pCNT and 5 mg sCNT to 5 mL ultrapure water and sonicating it for 10 min. In Figure 3-8A, both pCNT and sCNT were well dispersed in water right after sonication. Ten days after sonication, pCNT agglomerated and settled to the

bottom, while sCNTs remained dispersed in water for more than 3 months (Figure 3-8B). Because water is polar, it is reasonable that the hydrophobic pCNT cannot sustain good dispersion. Similar result was observed when DMSO was used as solvent. Both pCNT and sCNT dispersed well in DMSO after 3 minutes of sonication (Figure 3-8C); 10 hours later, pCNT again aggregated and settled to the bottom, while sCNT still had good dispersion (Figure 3-8D). These results confirm that sulfonation is an effective way to enhance the dispersibility of CNT in polar solvents and would facilitate the incorporation of sCNT into the polymer matrix.

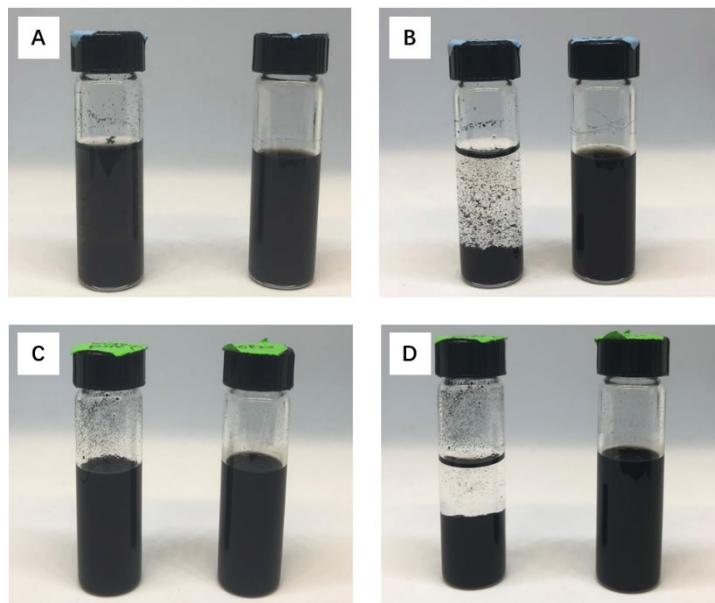


Figure 3-8. Dispersion test of sCNT and pCNT. A) 5 mg of pCNT (left) and sCNT (right) in 5 mL ultrapure water with 10-minute sonication; B) 10 days after sonication, pCNT (left) agglomerated and settled, while sCNT maintained good dispersion; C) 5 mg of pCNT (left) and sCNT (right) in 5 mL DMSO with 3-minute sonication; D) 10 hours after sonication, pCNT aggregates settled at the bottom while sCNT was still well dispersed.

3.2.3 Sulfonation result of Method 2

The XPS spectra of sCNT obtained by method 2 are presented in Figure 3-9 and Figure 3-10. In the full spectrum (Figure 3-9), two small peaks of sulfur and nitrogen are observed, in addition to two relatively large peaks of carbon and oxygen. In the detailed spectra, the C1s spectrum is decomposed into C=C (284.42 eV) and C-C and C-H (285.19 eV) (Figure 3-10a), which resembles the signal of pCNT and suggests that the elemental makeup of CNT was not changed. The oxygen peak in O1s spectrum is decomposed into C=O and S-O (530.63 eV) and C-O and S=O (531.566 eV), as is shown in Figure 3-10b. The sulfur peak and nitrogen peak are identified at 167.39 eV and 398.91 eV respectively (Figure 3-

10c and d, respectively). The presence of sulfur and nitrogen in spectra result shows that sulfonation of CNT by method 2 was successful.

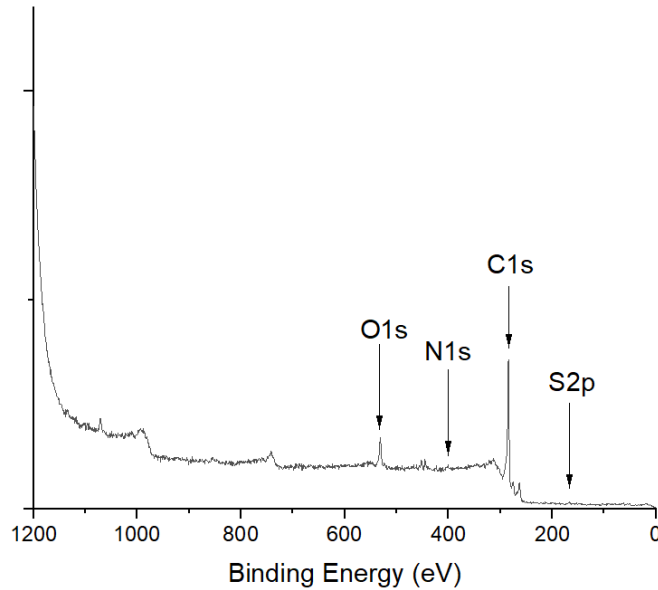


Figure 3-9. Full XPS spectrum of sCNT using method 2.

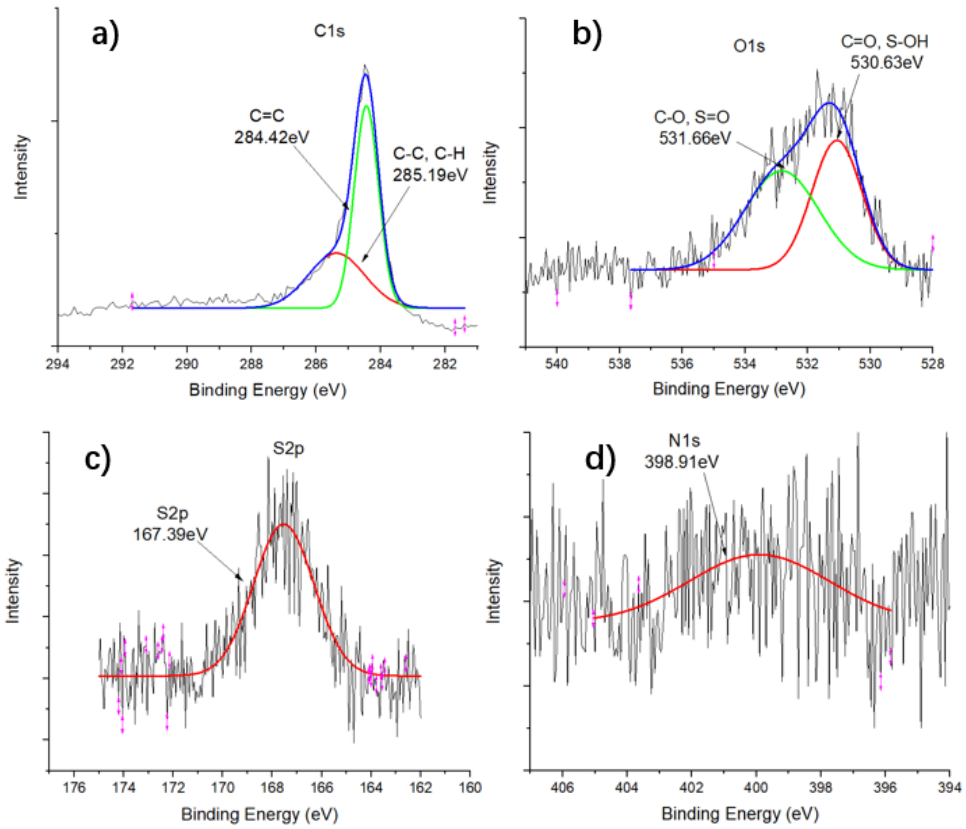


Figure 3-10. XPS detailed spectra of sCNT using method 2: a) C1s spectrum; b) O1s spectrum; c) S2p spectrum; d) N1s spectrum.

Similarly, the chemical composition of such sCNT could be calculated using corresponding relative sensitivity factors of each element (0.296 for C, 0.711 for O, 0.666 for S and 0.477 for N) (Moulder et al.) The result is summarized in Table 3-2 with data of pCNT as a comparison. However, the concentration of sulfur in sCNT in this case is around 2.8 w/w%, which is less than that of sCNT using method 1 (3.5 percent). Method 2 is expected to yield a higher sulfonation degree. Since method 1 is based on C-H defects, it is limited by available defects on the surface of pCNT. On the other hand, for method 2, the carboxylic group required for reaction is created by acid treatment before further conversion, as is mentioned in the protocol (Section 3.1.2). Therefore, the available reaction sites in method 2 are more controllable. To sustain the nanostructure of CNT, however, it may not be possible to oxidize pCNT excessively during acid treatment, especially considering that pCNT used in the experiment has multiple walls. Therefore, there is a practical limit for sulfonation degree using method 2. Nevertheless, method 2 is a useful platform for CNT functionalization. As illustrated in the protocol, method 2 is based on the amidation reaction between acyl chloride group from CNT and amine group from aminomethanesulfonic acid. By changing to different chemicals with the amine group, various functional groups can be tethered to the CNTs.

Table 3-2. Atomic composition of pCNT and sCNT using method 2.

Sample	Peak area				Atom ratio (C : O : S : N)	Weight percentage (C%:O%:S%:N%)	Ion- exchange capacity of -SO ₃ H (meq/g)
	C	O	S	N			
pCNT	13997	2557	-	-	1:0.076:0:0	90.8:9.8:0:0	-
sCNT	4264	1500	121	88	1:0.15:0.013:0.013	80.0:16.6:2.8:1.2	0.9

4 Nanocomposite ion exchange membrane fabrication and characterization

4.1 Nanocomposite IEM fabrication

4.1.1 Polymer functionalization

Poly(2,6-dimethyl-1,4-phenylene oxide) (PPO) (Sigma-Aldrich, analytical standard) was used as the backbone polymer of IEM with sulfonates as charge functional groups. To sulfonate PPO, 6 wt.% PPO was dissolved in chloroform by mechanical mixing for 30 minutes. Then, 8 wt.% chlorosulfonic acid solution (chloroform as solvent) was slowly added to the PPO solution over 30 minutes under vigorous stirring at room temperature, precipitating the sulfonated PPO. The volume ratio of PPO to chlorosulfonic acid solution was set at 1:1 to achieve the desired degree of functionalization. Sulfonated PPO polymer (sPPO) was then soaked and washed with ultrapure water and dissolved in methanol. The sulfonated PPO methanol solution was evaporated in a glass tray for 24 hours to form a thin film. To remove residual acid, the thin film was shredded into small pieces and washed with ultrapure water multiple times until the pH of the water was higher than 4. After washing, the polymer thin film was dried at room temperature for about 2 days.

4.1.2 Preparation of casting solutions

Sulfonated PPO polymer was dissolved in DMSO to obtain 19 wt% casting solutions. Then, sCNTs were mixed in the DMSO solution according to a certain weight percentage of total membrane weight. The sCNT-dispersed solution was immersed in an ultrasonic bath for 40 minutes before casting.

4.1.3 Membrane casting

The solvent evaporation method was employed for IEM fabrication. The polymer and carbon nanotube in DMSO solution was cast on a glass sheet using a casting knife set at about 1.0 mm, to yield an eventual membrane thickness of around 100 μm . The film was then dried in vacuum oven at 80° C for 24 hours and then at 95° C for another 24 hours to remove residual solvents. To obtain a membrane with different swelling degree, the heating time of 95° C was varied from 24 hours to 48 hours for some samples, and is furthered discussed in Chapter 5.

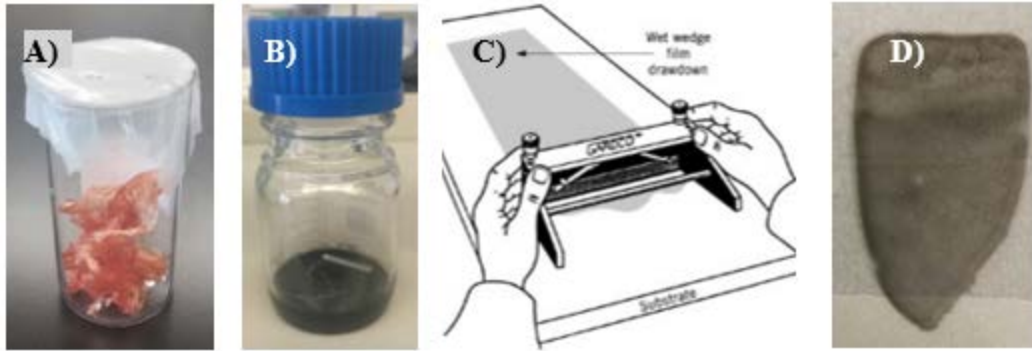


Figure 4-1. Experimental procedures of sCNT nanocomposite IEM fabrication: A) Sulfonated PPO polymer; B) Casting solution (sPPO and sCNTs in DMSO); C) spreading casting solution into a thin film with a casting knife; D) Nanocomposite cation exchange membrane.

4.2 IEM characterization

4.2.1 Ion-exchange capacity

Ion-exchange capacity refers to the total capacity of a membrane to hold exchangeable ions. For the cation exchange membrane (CEM), the acidity of protonated membrane sample is commonly used for ion-exchange capacity measurement. To protonate all the functional groups in the membrane, a sample membrane was immersed in 1 mol/L HCl solution for 24 hours and washed with deionized water. The membrane sample was then soaked in 50 mL of 1 mol/L NaCl aqueous solution for 24 hours. After soaking, 25 mL of the soaking solution was titrated with 0.01 mol/L NaOH using phenolphthalein as an indicator. The membrane sample was dried in vacuum oven at 60° C, about 760 mmHg for 24 hours. The weight of the dried membrane sample (W_{dry}) was recorded. The ion-exchange capacity was calculated with following equation (C_{NaOH} , V_{NaOH} for concentration and volume of NaOH solution in titration):

$$IEC = \frac{2 \times C_{NaOH} \times V_{NaOH}}{W_{dry}}$$

4.2.2 Swelling degree

Swelling degree defines the ability of the membrane matrix to absorb water. The wet membrane was soaked in ultrapure water for 24 hours. Then, it was patted dry with filter paper and the wet weight (W_{wet}) was recorded. The dry weight of the membrane (W_{dry}) was determined after 24 hour drying in a vacuum oven at 60° C, about 760 mmHg. Swelling degree was calculated using the equation below:

$$SD = \frac{W_{wet} - W_{dry}}{W_{wet}} \times 100\%$$

4.2.3 Membrane intrinsic resistivity/conductivity

An electrochemical test set-up based on a four-electrode cell system was used for resistance measurement (Figure 4-2A). A 3D-printed two-chamber cell (about 16 mL in each chamber) was separated by a membrane coupon of 2×2 cm effective area. The working electrodes in the two terminals of the cell were Pt-coated Ti mesh (4×4 cm). Two Ag|AgCl reference electrodes (BASi RE-5B, West Lafayette, In.), positioned 7 mm apart, measured the potential difference across the membrane. Figure 4-2B shows the testing set-up.

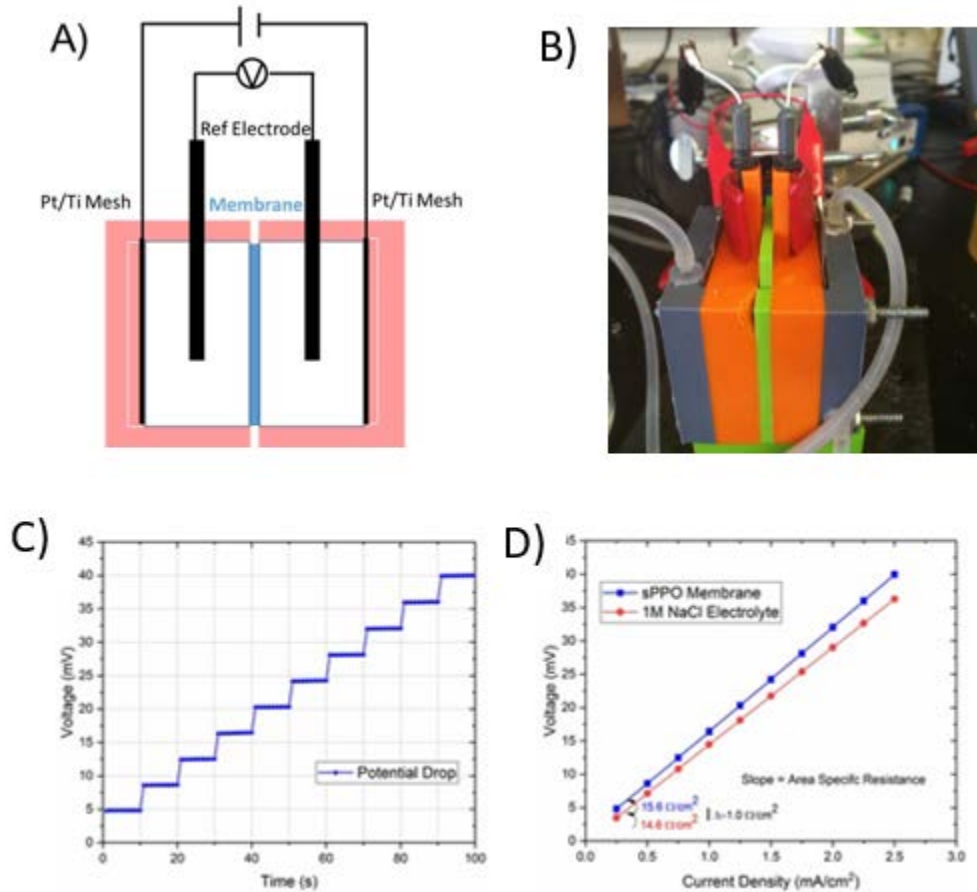


Figure 4-2. Experimental methods for membrane resistance/conductance measurements: A) Schematic of the four-electrode test; B) Membrane resistance test cell; C) Voltage response for different constant current steps; D) Representative plot of membrane resistance calculation.

Membrane resistance tests were conducted using an electrochemical workstation (Interface 1010E, Gamry, Penn.). The test cell was filled with 1 mol/L NaCl electrolyte solution. Direct current was applied, ranging from 0.001A-0.010A (0.25 mA/cm² to 2.5 mA/cm²), and voltage drop across the membrane was recorded. Each current step was maintained for 10 seconds and the voltage drop was sampled 10 times. Resistance of the membrane was calculated as the difference between slopes of voltage drop as a function of current density with

and without membrane, as is shown in Figure 4-2D. The wet thickness of the membrane was measured with a micrometer. The resistance of membrane normalized by membrane thickness yielded the membrane intrinsic resistivity (reciprocal of conductivity).

4.2.4 Membrane permselectivity

Permselectivity describes the selectivity of the IEM for counterion transport. The same cell system and electrochemical workstation employed for resistance characterizations were used for permselectivity measurement. The static method was adopted, which determines permselectivity from the potential difference across the membrane separating two solutions of different concentrations. In this study, 0.1 mol/L NaCl was circulated on one side of the film, and 0.5 mol/L NaCl was circulated on the other side. The potential difference was measured with two Ag|AgCl reference electrodes (BASi RE-5B, West Lafayette, In.) plugged into the two chambers. The potential between the reference electrodes was tracked as a function of time until the potential stabilized at $\psi_{measured}$. Theoretical Nernst potential ($\psi_{theoretical}$) of 0.5 to 0.1 mol/L NaCl was calculated as 38mV. The apparent permselectivity was determined using the following equation, and Figure 4-3 shows the schematic diagram of the permselectivity tests.

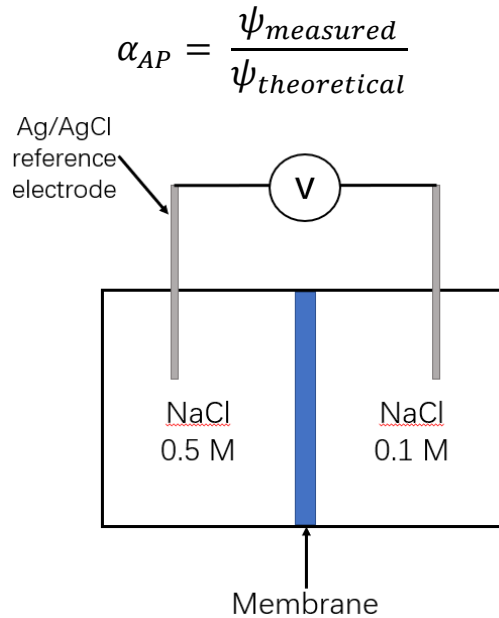


Figure 4-3. Schematic diagram of permselectivity test.

4.2.5 Scanning electron microscopy imaging

To prepare the samples mimicking the swollen state, the fabricated IEM coupons were soaked in 1 mol/L NaCl for at least 24 hours. The water-swollen membranes were then dipped into liquid nitrogen for about 40 seconds. The membrane

samples were then broken by tweezers to expose the cross-section for imaging. The samples were mounted onto scanning electron microscopy specimen holders with carbon tape. To eliminate the static electric charge effect, about 10 nm Au coating was applied onto the samples before imaging. The samples were characterized by scanning electron microscopy (Zeiss SIGMA VP).

4.3 Results and discussion

4.3.1 Nanocomposite with lab-functionalized sCNTs

Sulfonated CNTs functionalized by the acetyl sulfuric acid method (Method 1) were used for nanocomposite IEM fabrication (referred to as lab-functionalized sCNTs). These sCNTs offer an equivalent $-\text{SO}_3\text{H}$ capacity of about 1.1 meq/g. The nanocomposite IEMs with lab-functionalized sCNTs are fabricated and characterized to determine ion-exchange capacity, swelling degree, ASR, apparent permselectivity, α_{ap} , and wet thickness, l . Further, membrane intrinsic resistivity, ρ , is determined by normalizing ASR by l and is an intensive property of the IEM (i.e., independent of dimensions and amount of material).



sCNT weight percent	0 w/w%	2.0 w/w%	10 w/w%	20 w/w%
Thickness, l [μm]	86 ± 7	75 ± 8	105 ± 3	98 ± 5
IEC [meq/g]	1.60	1.54	1.50	1.48
SD [%]	32.5	42.3	33.9	44.9
ASR [Ωcm^2]	1.39 ± 0.04	1.21 ± 0.06	1.31 ± 0.03	1.19 ± 0.04
ρ [Ωcm]	163 ± 5	161 ± 8	125 ± 3	122 ± 4
α [-]	1.037	1.033	1.037	1.016

Figure 4-4. l , ion-exchange capacity, swelling degree, ASR, ρ and α of the fabricated membranes (with lab-functionalized sCNTs).

Greater incorporation of sCNTs resulted in larger wet thickness of the fabricated IEMs, despite equivalent or slightly lower swelling degrees (Figure 4-4). This corroborates with the micro-domains of void space observed in the scanning electron microscopy micrographs (Figure 4-5, discussed later). Ion-exchange capacity and swelling degree of membranes with different formulations are similar within each batch and, in general, are within the range reported in literature. Apparent permselectivity of the fabricated membranes is also effectively not influenced by the amount of sCNTs (small differences in measured α of the IEMs are within experimental variation of the characterization method). Figure 4-2 shows a decreasing trend in intrinsic resistivity of the nanocomposite

membranes with an increasing amount of sCNT incorporation. For example, 23 percent and 25 percent reduction in resistivity are attained for 10 and 20 w/w%, respectively (Figure 4-5). Meanwhile, apparent permselectivity is about 1.02 to 1.03. Due to the junction potential of Ag|AgCl reference electrodes, the apparent permselectivity of cation exchange membranes can be higher than unity if measured by the static method.

Therefore, the nanocomposite IEMs achieved enhanced ionic conductivity without noticeable compromise in counterion selectivity. Further analysis of the conductivity-permselectivity trade-off is presented in Chapter 5.

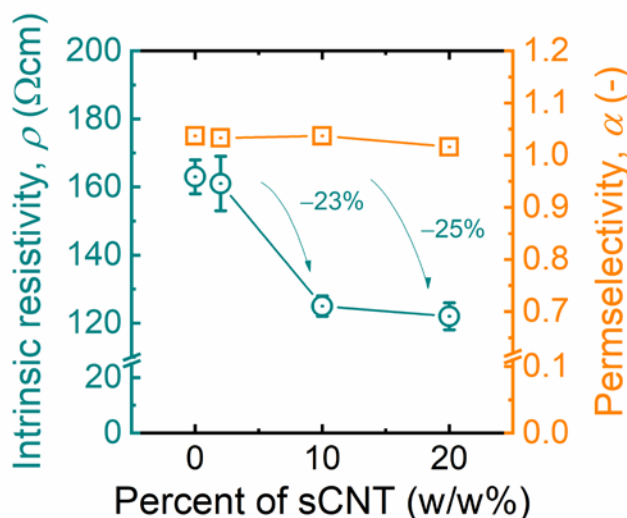


Figure 4-5. Intrinsic resistivity, ρ , as a function of weight percent of lab-functionalized sCNTs in IEM; and permselectivity, α , which is effectively independent of sCNT addition.

4.3.2 Nanocomposite with commercial sCNTs

Commercial sCNTs purchased from commercial manufacturer Cheap Tubes Inc. (Cambridgeport, Vt.) are used to fabricate nanocomposite IEMs. The equivalent $-\text{SO}_3\text{H}$ capacity is about 0.02-0.29 meq/g, calculated from material specs provided by the manufacturer. The sulfonation degree of commercial sCNTs is much lower than the lab-functionalized sCNTs, and commercial sCNTs are also less stable in DMSO solvent.

The trends of membrane characteristics of the commercial-sCNTs incorporated cation exchange membrane are similar to the CEMs with lab-functionalized sCNTs. Reductions in resistivity of 18 percent and 29 percent are attained for 10 and 20 w/w%, respectively (Figure 4-5). Apparent permselectivity is about 0.87 to 0.89. The lower apparent permselectivity compared to CEMs with lab-functionalized sCNTs (1.02 to 1.03) is attributed to the lesser degree of functionalization. Additionally, the lower functionalization degree also affected

the sCNT dispersion and eventual membrane morphology (discussed later). The finding highlights the importance of CNT functionalization for nanocomposite IEM performance.

Commercial sCNT				
sCNT weight percent	0 w/w%	2.0 w/w%	10 w/w%	20 w/w%
Thickness, l [μm]	44.0 ± 1.3	44.6 ± 3.6	54.6 ± 1.4	57.2 ± 3.2
IEC [meq/g]	2.17	2.29	2.21	2.15
SD [%]	69.9	80.6	71.8	56.9
ASR [Ωcm^2]	0.54 ± 0.09	0.54 ± 0.06	0.52 ± 0.09	0.52 ± 0.05
ρ [Ωcm]	122 ± 21	122 ± 7	100 ± 9	87 ± 4
α [-]	0.874	0.894	0.890	0.878

Figure 4-6. l , ion-exchange capacity, swelling degree, ASR, ρ and α of the fabricated membranes (with commercial sCNTs).

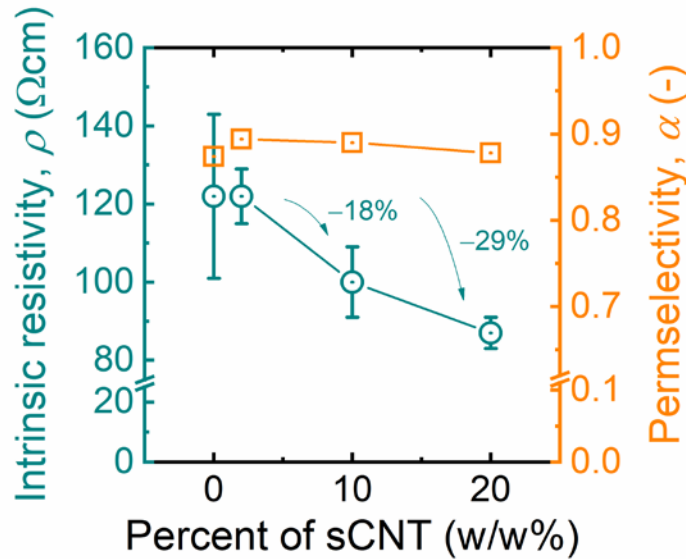


Figure 4-7. Intrinsic resistivity, ρ , as a function of weight percent of commercial sCNTs in IEM; and permselectivity, α , which is basically independent on sCNT addition.

4.3.3 Morphology of nanocomposite IEMs

The surface and cross-section of the nanocomposite IEMs with 0, 10, and 20 w/w% lab-functionalized sCNTs are imaged using scanning electron microscopy. Figure 4-6 shows the cross-section structure of pristine IEM (i.e., 0 percent carbon nanotubes). Small shreds of polymer observed in the low magnification image (Figure 4-6A) are artifacts of sample preparation when the membrane is

broken to expose the cross-section. Across all magnification, the dense morphology of the polymer structure is clearly visible for the surface and cross-section.

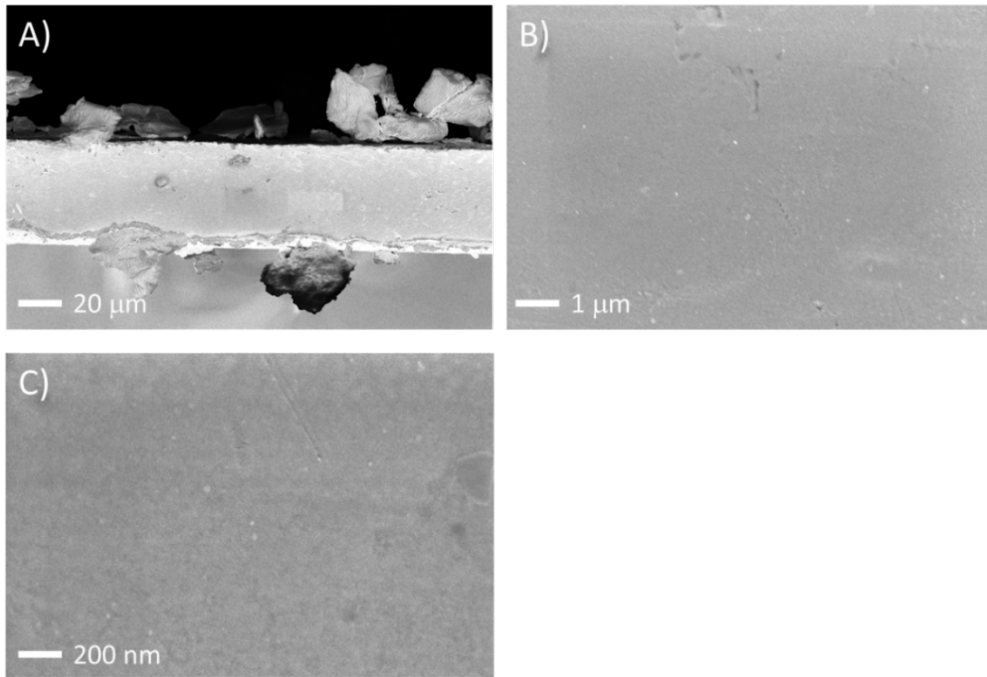


Figure 4-8. 0 w/w% sCNTs IEM cross-section: A) $\times 500$ magnification, B) $\times 10,000$ magnification, C) $\times 50,000$ magnification

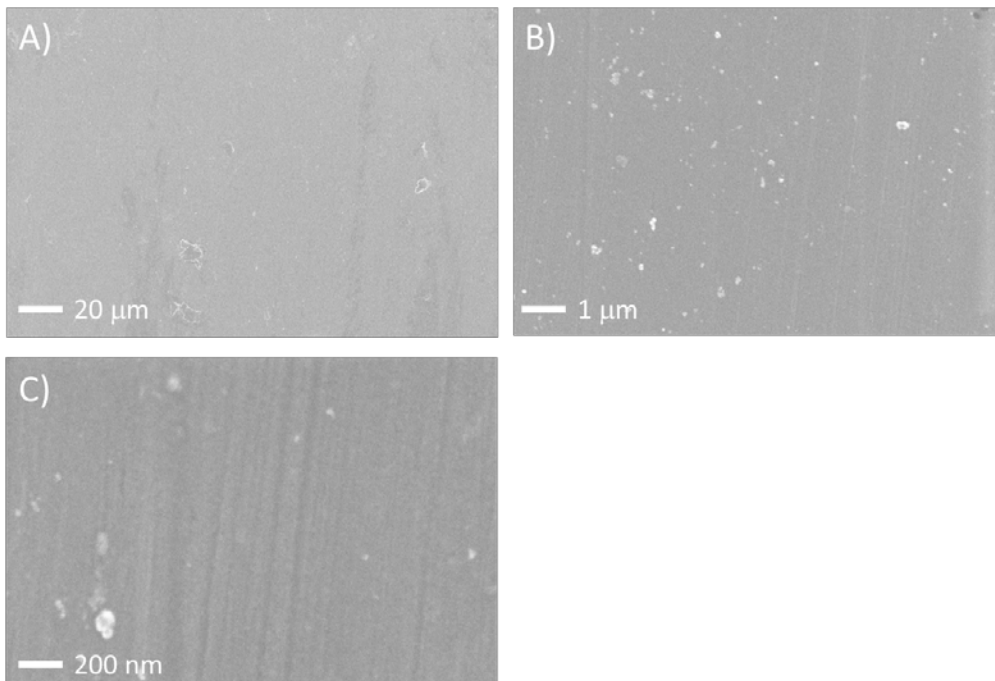


Figure 4-9. 0 w/w% sCNTs IEM surface: A) $\times 500$ magnitude, B) $\times 10,000$ magnitude, C) $\times 50,000$ magnitude

The dense morphology is preserved in the polymer matrix of the 10 w/w% sCNT membranes (Figures 4-8 to 4-10), but CNTs are visible in the membrane, especially in the cross-sectional micrographs. The electrically conducting CNTs are indicated by bright rods and spots in Figure 4-8B and C. The width of the rods is measured to be 26.98 nm, corresponding well with the diameter of CNTs based on manufacturer's specs (20 to 30 nm). The generally even distribution of the bright rods and spots indicate that the CNTs are well dispersed within the polymer matrix of the nanocomposite IEM.

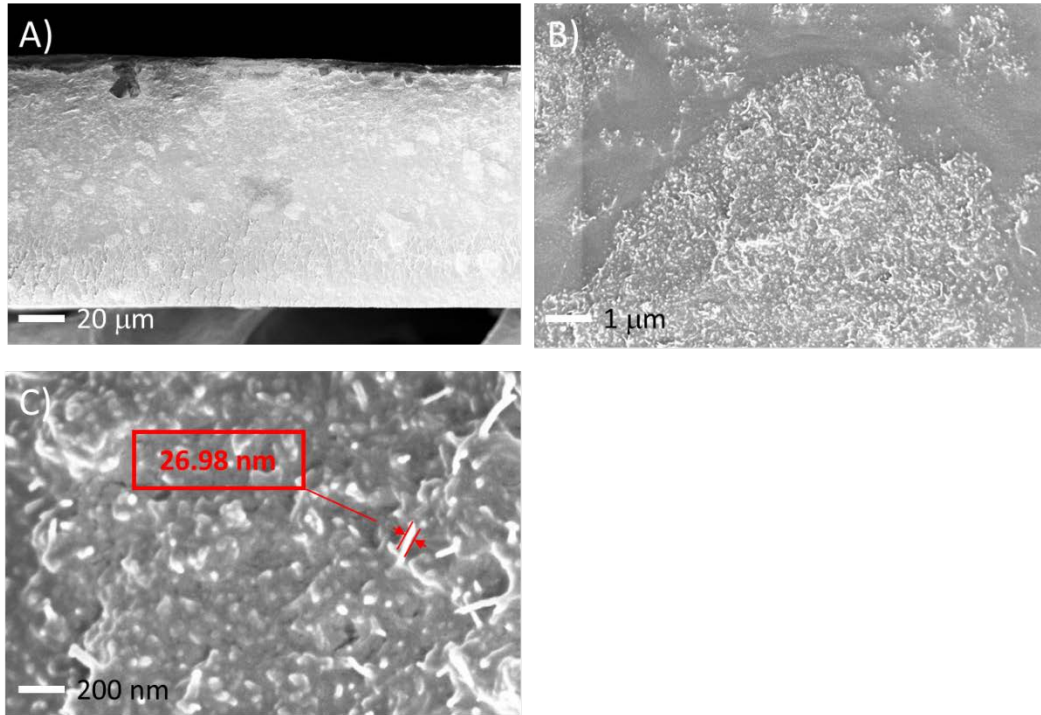


Figure 4-10. 10 w/w% sCNTs IEM cross-section: A) $\times 500$ magnification, B) $\times 10,000$ magnification, C) $\times 50,000$ magnification

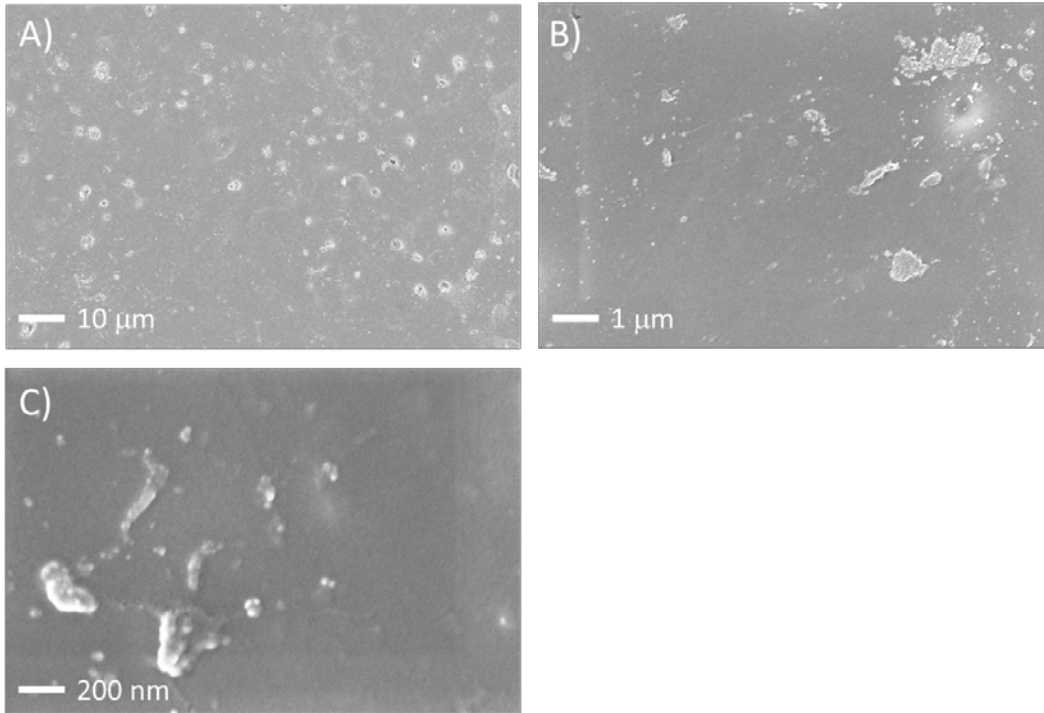


Figure 4-11. 10 w/w% sCNTs IEM surface, top view: A) $\times 1000$ magnification, B) $\times 10,000$ magnification, C) $\times 50,000$ magnification

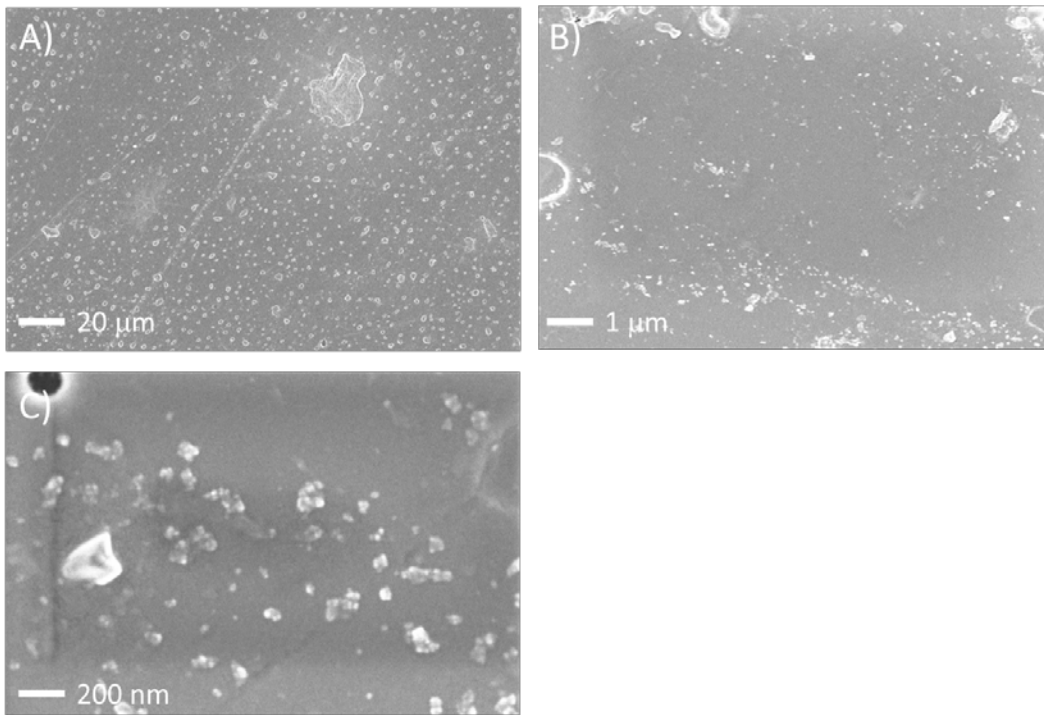


Figure 4-12. 10 w/w% sCNTs IEM surface, bottom view: A) $\times 500$ magnification, B) $\times 10,000$ magnification, C) $\times 50,000$ magnification

The surface roughness of 10 percent sCNT IEM is considerably higher than the pristine membrane. However, only a few bright spots are observed on the surface, indicating the CNTs are well embedded in the polymer matrix. The different in roughness between the top and bottom surfaces is attributed to the solvent evaporation process: the top surface is exposed to the environment while the bottom surface is in contact with the glass substrate.

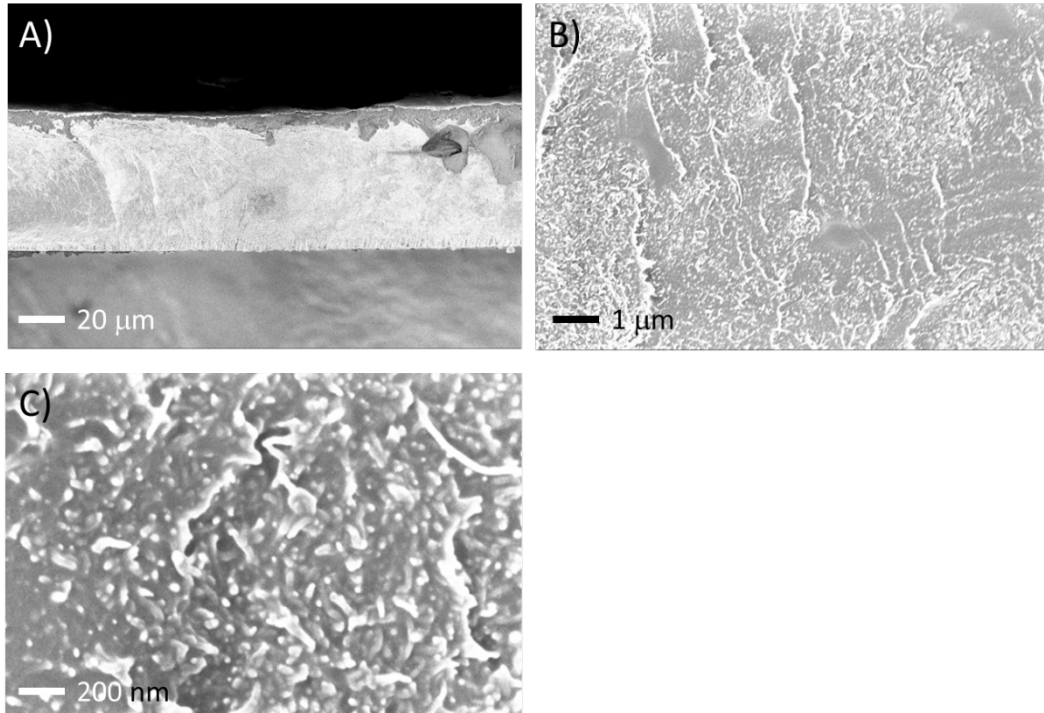


Figure 4-13. 20 w/w% sCNTs IEM cross-section: A) ×500 magnification, B) ×10,000 magnification, C) ×50,000 magnification

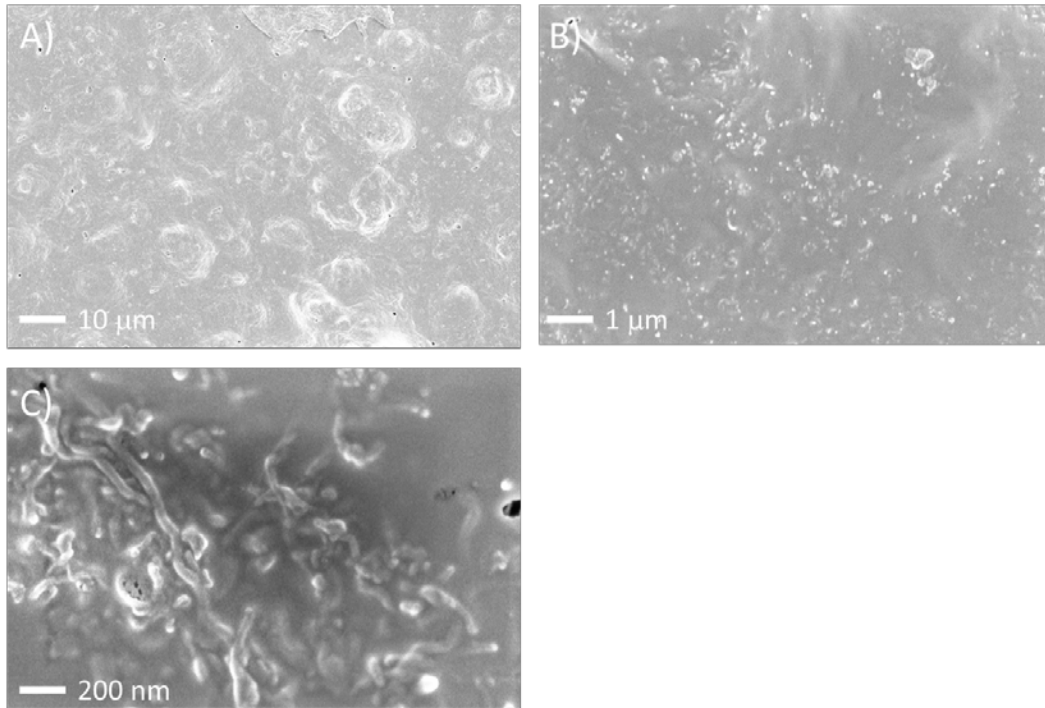


Figure 4-14. 20 w/w% sCNTs IEM surface, top view: A) $\times 1000$ magnification, B) $\times 10,000$ magnification, C) $\times 50,000$ magnification

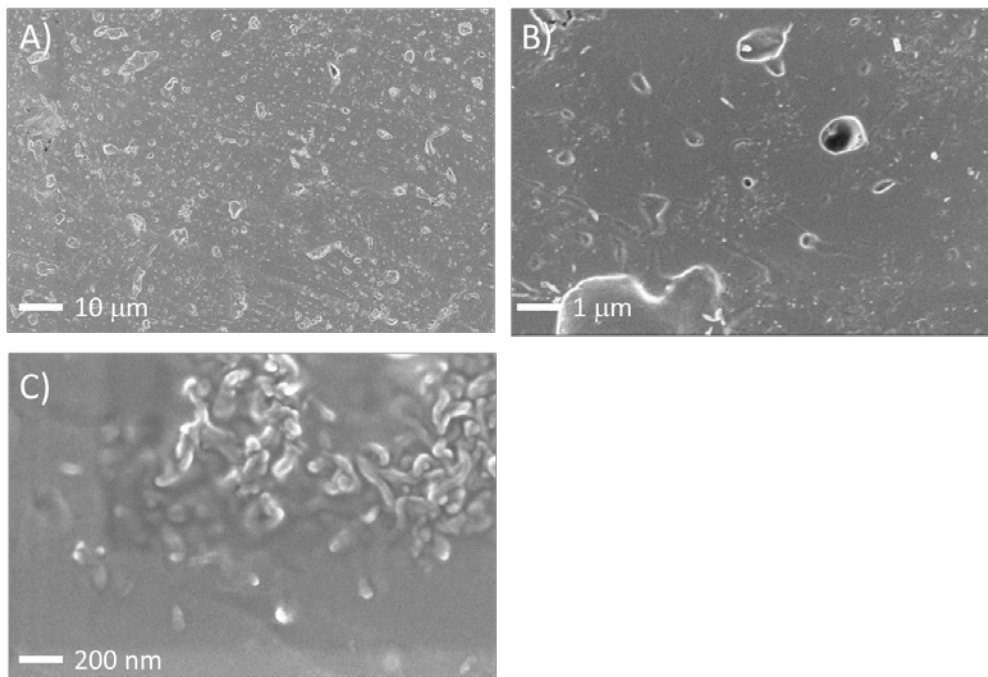


Figure 4-15. 20 w/w% sCNTs IEM surface, bottom view: A) $\times 1000$ magnification, B) $\times 10,000$ magnification, C) $\times 50,000$ magnification

The 20 w/w% sCNT IEM samples show similar features. As expected, more CNTs are observed in the cross-section micrograph (bright rods and spots in

Figure 4-11). Due to a higher dosage of sCNTs, the roughness of the top-side surface is also higher (Figures 4-12 and 4-13). However, the height of the roughness unevenness is on the order of micrometers, is evenly distributed over the membrane, and is effectively smooth during visual inspection.

5 Impacts of sCNT incorporation on the conductivity-permeability trade-off

This chapter examines the conductivity and permselectivity of the nanocomposite IEMs with a range of swelling degree, by varying the solvent evaporation heating time (described in Section 4.1). Here, lab-functionalized sCNTs are employed for membrane fabrication.

5.1 Resistivity reduction from incorporation of sCNT

As discussed in Chapter. 2, conductivity is positively related to swelling degree, whereas resistivity (reciprocal of conductivity) and swelling degree are negatively related. IEMs with a range of swelling degree were fabricated and their resistivity measured. The results are shown in Figure 5-1 for sCNT-incorporated and control membranes (0 and 20 w/w%, respectively). For both sets of IEMs, the resistivity rose sharply at low swelling degree. Conversely, when swelling degree was large, the resistivity of both nanocomposite IEMs and pristine IEMs dropped significantly. Comparing the trendlines, it is apparent that incorporating sCNT into the polymer matrix yields lower resistivity for the same swelling degree (i.e., shifts the swelling degree-intrinsic resistivity trend lines toward the bottom left). In addition, enhancement in conductivity is more pronounced at lower swelling degree.

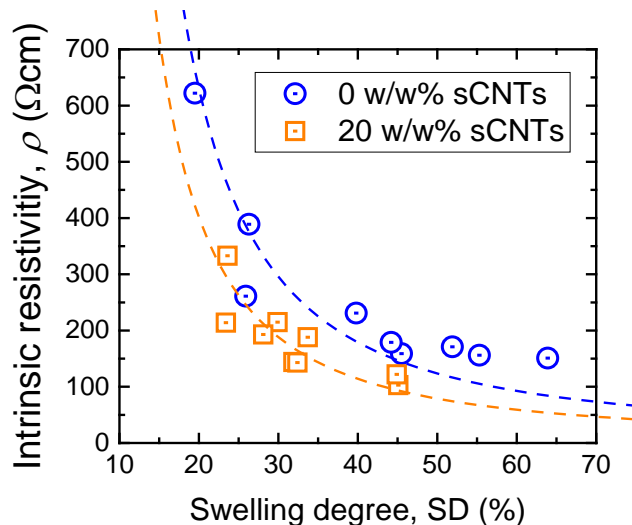


Figure 5-1. Intrinsic resistivity, ρ , as a function of swelling degree, for sCNT-incorporated and control membranes.

The results also validate the transport model presented in Chapter 2. The behavior of resistivity as a function of swelling degree according to the transport model are

indicated by the dashed lines. The simulated trend agrees well with the experimental results, as evident by the general good fitting.

5.2 Advancing conductivity-permselectivity trade-off

Results presented in Chapter 4 show that conductivity is improved (up to about 25 percent) with the incorporation of sCNT, while permselectivity is not significantly changed. The improvement in permselectivity-conductivity is more clearly displayed in Figure 5-2. The trendlines of both the sCNT-incorporated and control IEM exhibit a negative slope, as described by the transport model presented earlier. Incorporating sCNT into the CEM polymer matrix shifts the conductivity-permselectivity trendline outward, to the top right. This demonstrates the potential of using nanomaterials to advance the conductivity-permselectivity trade-off governing conventional IEMs.

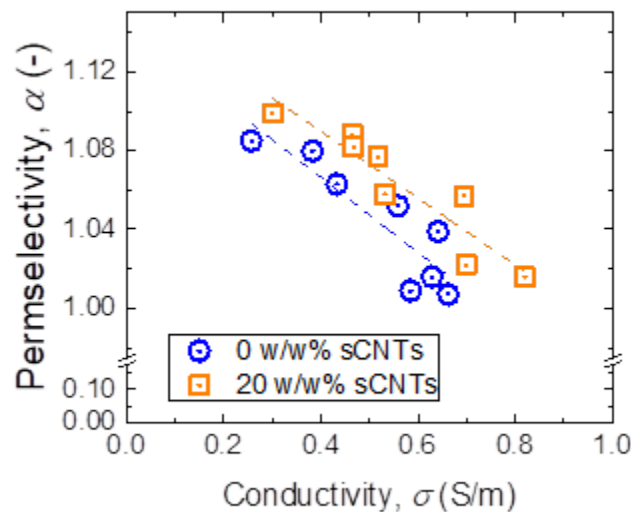


Figure 5-2. Permselectivity as a function of conductivity for 0 and 20 % sCNT in sPPO IEM.

We postulate that the improved conductivity-permselectivity of the fabricated nanocomposite IEMs is due to altered morphology of the membrane that facilitated enhanced ion transport. The contiguous and interconnected network of CNTs across the nanocomposite IEM thickness favorably shortens the effective transport pathway for ions. For the conventional IEMs, the polymer chains are intertwined to form a compact cluster (Figure 5-3). The CNTs embedded in the polymer matrix disrupt the compact polymer packing, loosening the structure to create shortcuts for ion electro-diffusion. Thus, the transport pathway is less tortuous and the effective ion diffusivity is correspondingly improved.

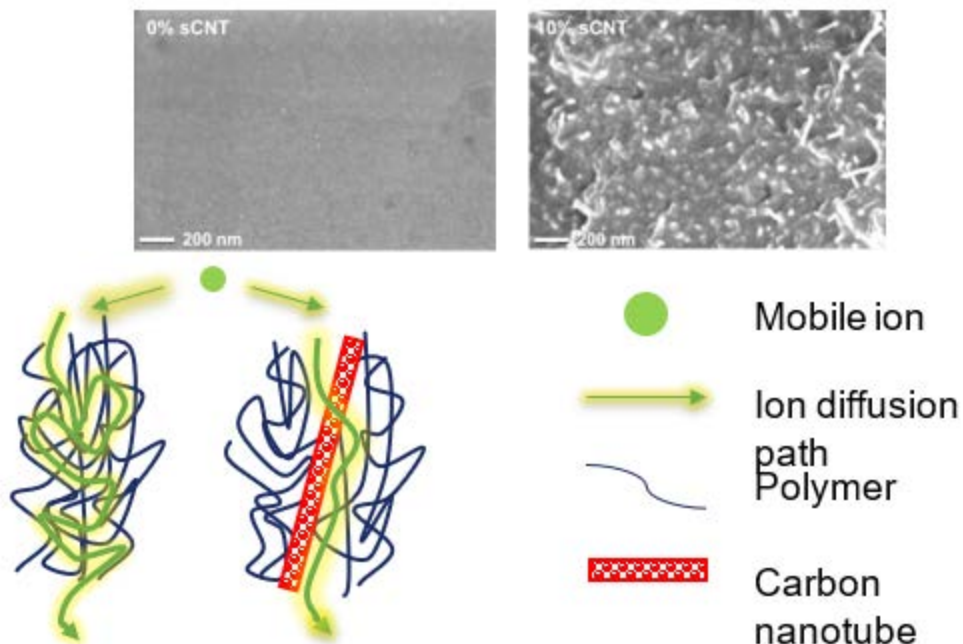


Figure 5-3. Schematic of posited ion transport in pristine and nanocomposite IEM.

Permselectivity, on the other hand, is not significantly impacted by the CNT incorporation. We conjecture that the sulfonic acid moieties functionalized onto the CNTs contribute to the ion-exchange capacity /fixed charge density. Hence, the charge exclusion effect of the nanocomposite membrane is preserved and selectivity for counterions is not detrimentally affected.

This study shows that the thoughtful incorporation of one-dimensional nanomaterial into the polymer matrix to form a percolating network is a promising platform for improving the conductivity and permselectivity performance of IEMs. The principles, methodologies, and findings have significant implications for the application of other nanomaterials with different functionality to attain better-performing IEMs.

6 Electrodialysis stack test and performance assessment

6.1 Methods

An IEM stack with membrane effective area of $4 \times 4 \text{ cm}^2$ was fabricated by laser cutting and 3D printing (Figure 6-1A). The stack operates with two electrode chambers and one pair of flow channels, a concentrate channel with high concentration (HC) and a diluate channel with low concentration (LC). Two graphite sheets were used as working electrodes, and 0.1 mol/L NaCl was used as the feed electrolyte solution. The concentration of feed solution simulates

brackish water (about 6,000 ppm TDS). The feed solutions were recirculated through the LC and HC chambers, which mimics co-current operation of membrane stack. Electrode rinse solution (1 mol/L NaCl + 0.05 mol/L $K_3[Fe(CN)_6]$) was also recirculated in a closed loop to convert between ionic and electric currents. In electrodialysis (ED), the electrochemical workstation (Interface 1010E, Gamry, Penn.) applied a constant electric current across the ion exchange membrane stack to drive the ion transport. Two 10 w/w% sCNT (lab-made) CEMs and one commercial AEM from Selemion AMV (AGC Engineering Co., Ltd.) were installed in the stack for the ED desalination test. The concentration of LC was measured using a conductivity meter. In the control test, sCNT CEMs were replaced by commercial CEMs from Selemion CMV (AGC Engineering Co., Ltd.).

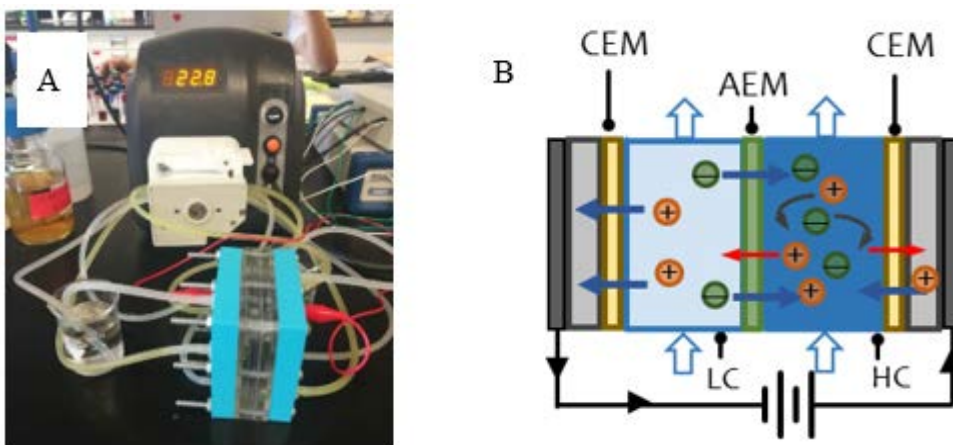


Figure 6-1. Design of the ED stack: A) operation of the ED stack, B) schematic of the stack, with the arrows indicating the direction of electric current or cation (+) and anion (-) permeation. CEMs and AEM separate diluate (LC) and concentrate (HC) flow channels. The electrode rinse solution is also circulated between electrode chambers (light gray chamber).

6.2 Nanocomposite IEM desalination

In the ED experiment with nanocomposite IEMs, a 60 mL electrolyte solution was recirculated in each feed channel. The constant applied current was set at 60 mA, equivalent to a current density of 3.75 mA/cm^2 . As shown in Figure 6-2, the stack voltage increased as the LC chamber was gradually desalinated and the conductivity dropped sharply. The drop in salinity of the LC solution matched the constant current operation. After 2.5 hours, the LC concentration fell below $17 \times 10^{-3} \text{ mol/L}$ (1,000 ppm TDS, WHO drinking water guideline) from $100 \times 10^{-3} \text{ mol/L}$, verifying that the fabricated nanocomposite CEMs were functional.

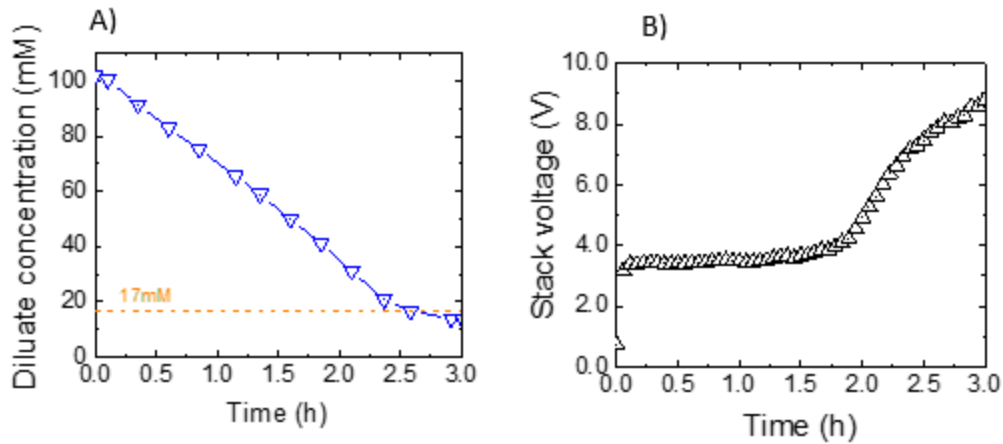


Figure 6-2. ED operation of IEM stack with 10 w/w% sCNT CEM. A) Concentration of diluate channel (LC) as a function of time, and B) stack voltage across two end electrodes.

The current efficiency (CE) of ED desalination process is:

$$CE = \frac{\Delta CV}{tIF}$$

where ΔC is the concentration drop of the diluate channel, V is the volume of diluate electrolyte solution, t is time, I is the electric current, and F is the Faraday constant (96485 sA/mol). The CE fraction of electric current was used to drive counterion transport, rather than co-ion permeation. Thus, CE is a measure of selectivity and also characterizes the efficiency of electric current use. The energy efficiency of ED desalination is therefore directly impacted by CE. An average CE of 85 percent was achieved during the desalination duration.

6.3 Desalination results with commercial IEM

Desalination of simulated brackish water is carried out with commercial cation exchange membranes. Since the resistance of commercial CEM is higher than the resistance of the fabricated nanocomposite CEMs, the stack resistance with commercial CEMs is larger. To avoid voltage overload (more than 10V) of the electrochemical workstation for this ED experiment, the constant applied current was reduced to 40 mA, an equivalent current density of 2.5 mA/cm². Fifty mL of electrolyte solution was recirculated in each feed channel. Similar to the results with nanocomposite IEMs, the stack voltage also increased as the LC chamber was gradually desalinated, and the conductivity dropped sharply. Due to the constant current applied, a linear drop in salinity of the diluate channel is observed. After 3.2 hours, the LC concentration dropped below 17×10^{-3} mol/L, from 100×10^{-3} mol/L.

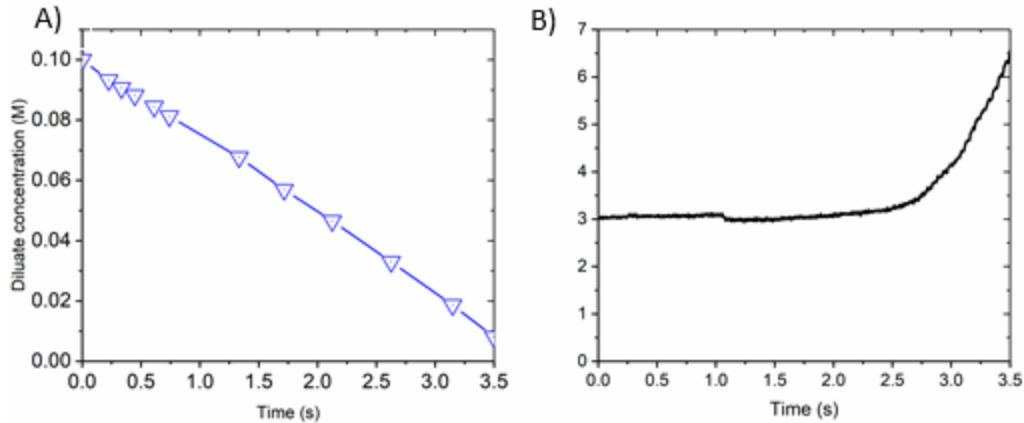


Figure 6-3. ED operation of the IEM stack with commercial CEM. A) Concentration of diluate channel (LC) as a function of time, and B) stack voltage across two end electrodes.

The commercial and lab-cast nanocomposite cation exchange membranes showed similar trends in stack voltage and LC channel concentration profile. The average current efficiency of the ED desalination with commercial IEM is 88 percent, comparable with the sCNT-incorporated CEMs. In the laboratory-scale stack tests, a low number of membrane pairs were employed (1.5 in this setup). For actual ED operation, a much larger number of membrane pairs and chambers are used, and higher current efficiency can be obtained.

6.4 Energy requirement assessment

Specific energy requirement is the energy to produce a unit volume of fresh product water. It impacts the cost effectiveness and competitiveness of ED desalination. The energy requirement with nanocomposite IEMs is assessed and compared to conventional membranes to project the potential energy savings. The following assumptions and conditions are adopted:

- 1) The feed stream of 100×10^{-3} mol/L NaCl is desalinated to 17×10^{-3} mol/L target concentration. The flow rate ratio of LC and HC is 1:1.
- 2) Based on the experimental stack test results, the ED current efficiency is conservatively set at 85 percent for both membranes. Operating electric current density is set at 3.75 mA/cm^2 , a common operating current density.
- 3) The contribution of the redox couple and end electrodes are neglected because an actual ED stack uses a large number of cell pairs.
- 4) Membrane resistance and permselectivity is assumed to be constant as the bulk concentrations varies during the desalination process. Since the scale of concentration change is below 0.2 mol/L in brackish water desalination, the variation of those membrane properties is not significant, justifying this simplifying assumption. The analysis in Chapter 2 further substantiates this.

- 5) The assessment considers that a 25 percent decrease in resistance is achieved by the nanocomposite membranes over conventional IEMs (approximate performance of 10 w/w% sCNT IEMs). This is a conservative estimate, as the reduction in resistivity likely can be enhanced with further optimization of the fabrication parameters. Area specific resistance of 10 to 15 Ωcm^2 is examined for the conventional IEMs.
- 6) The following typical dimensions for the stack design are adopted in this assessment: the chamber height of the HC and LC channel is 100 μm , and the spacer in the flow channel leads to a shadow effect factor of 0.8.

The stack voltage, including both ohmic voltage drop and Nernst potential of the IEMs, is determined as a function of time. The specific energy of desalination is then obtained by integrating the product of voltage and current (i.e., power) across the desalination duration. Projected energy savings of 13.3 to 15.8 percent are achieved with enhanced conductivity of the nanocomposite IEMs (Figure 6-4), demonstrating that the use of nanocomposite IEM can reduce the energy consumption of ED desalination. Further optimization can be explored to improve the performance of nanocomposite IEMs in ED stacks.

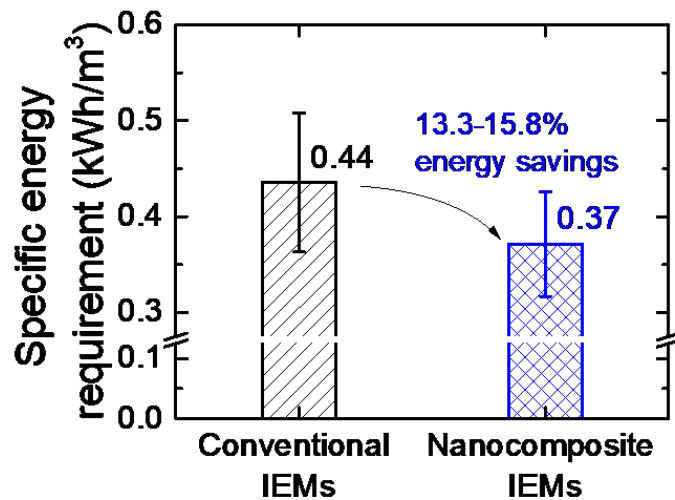


Figure 6-4. Projected specific energy requirement of ED desalination with conventional and nanocomposite IEMs.

7 Concluding remarks

7.1 Summary of project outcomes

The overarching aim of this project is to develop nanocomposite IEMs with enhanced conductivity and permselectivity for ED desalination. An analytical study was conducted to better understand the structure-property-performance relation of IEMs, and an experiment was carried out to develop nanocomposite IEMs and demonstrate their improved performance. A summary of the key findings is listed below:

- An IEM transport model is presented that uses the Nernst-Planck framework and counterion condensation theory. The model indicates that the permselectivity-conductivity trade-off is mainly driven by IEM water sorption. Increasing membrane ion-exchange capacity and reducing thickness can yield highly selective and conductive IEMs.
- The functionalization of carbon nanotubes with sulfonic acid moieties was shown and the fabrication of nanocomposite cation exchange membranes was demonstrated. The sulfonated carbon nanotubes were incorporated into sulfonated poly(p-phenylene oxide) polymer matrix with a range of loading (0 to 20 w/w%).
- The fabricated nanocomposite IEMs exhibited improved conductivity while maintaining permselectivity. Intrinsic resistivity was favorably lowered by 25 to 29 percent, with up to 20 percent incorporation of sCNT. Enhancement in conductivity was more pronounced for membranes with lower swelling degree. The nanocomposite fabrication strategy shows promising potential to advance the permselectivity-conductivity trade-off of conventional IEMs and achieve unprecedented performance.
- ED desalination of brackish water (simulated by 100×10^{-3} mol/L NaCl solution) to drinking water standards (less than 1,000 ppm TDS) was demonstrated with the fabricated nanocomposite membranes.

The energy requirement assessment projects that the energy savings of about 13.3 to 15.8 percent is achievable with nanocomposite membranes.

7.2 Recommended next steps

Further studies can further optimize the performance of nanocomposite IEMs. For example, the effect of ion-exchange capacity, nanotube diameter, length and aspect ratio, functionalized charged group on IEM conductivity, and permselectivity can be investigated. The nanocomposite IEM fabrication platform developed in this project can be further extended to other nanomaterials, such as

nano-dots, -wires, and -sheets. Additional optimization can be pursued at a process level to reveal more insights on ED operation with nanocomposite IEM. Actual brackish water feed streams for ED desalination are complex solutions with a multitude of components, whereas this study only focused on investigating simulated solutions consisting of NaCl. Future studies should characterize the conductivity enhancement of the fabricated nanocomposite IEMs with solutions that are more representative of actual brackish water (i.e., contains other ions such as Ca^{2+} , Mg^{2+} , CO_3^{2-} , SO_4^{2-} , and silica).

7.3 Research products

7.3.1 Publications

- 1) Fan, H. and Yip, N.Y., “Elucidating conductivity-permselectivity trade-offs in electrodialysis and reverse electrodialysis by structure-property analysis of ion-exchange membranes,” *Journal of Membrane Science*, March 2019, Volume 573, 668–681. [doi.org:10.1016/j.memsci.2018.11.045](https://doi.org/10.1016/j.memsci.2018.11.045)
- 2) Fan, H., Huang, Y. and Yip, N.Y., “Advancing Conductivity-Permselectivity Trade-off of Ion-Exchange Membranes with Sulfonated CNT Nanocomposites,” *Journal of Membrane Science*, manuscript in preparation.

7.3.2 Conference presentations

- 1) Yip, N.Y., and Fan., H., “Structure-Property Analysis of Conductivity-Permselectivity Trade-off in Ion-Exchange Membranes,” 254th ACS National Meeting & Exposition, Washington, D.C., August 2017.
- 2) Fan, H., Huang, Y. and Yip, N.Y., “Advancing Conductivity-Permselectivity Trade-off of Ion-Exchange Membranes with Sulfonated CNT Nanocomposites,” North American Membrane Society 28th Annual Meeting, Pittsburgh, Penn., May 2019.

Appendix – Model Development

In this section, the transport model for ion permeation in IEMs is presented and key equations are listed. The model considers the solution-membrane interface to be at electrochemical quasi-equilibrium and uses the modified Nernst-Planck equation to describe ion fluxes within the membrane matrix under an electrochemical potential gradient. Counterion condensation theory is employed to determine ion activity and diffusion coefficients within the membrane matrix. Membrane performance parameters in ED and RED are then introduced and their significance is discussed.

Equilibrium concentrations at solution-membrane interface

Figure A-1 shows an IEM of homogenous fixed charge density, $c_{\text{fix}}^{\text{m}}$ (dotted horizontal green line), separating high and low concentration solutions of $c^{\text{s,HC}}$ and $c^{\text{s,LC}}$, respectively. At equilibrium at the solution-membrane interfaces, the electrochemical potential, $\bar{\mu}_i$, of species i = counterions, co-ions, (or water) in solution and membrane are equal:

$$\bar{\mu}_i^{\text{m}} = \bar{\mu}_i^{\text{s}} \quad (1)$$

where superscripts m and s denote membrane and solution phase, respectively. The electrochemical potential is the sum of the chemical potential, μ_i , and the electrical potential, $\bar{\mu}_i = \mu_i + z_i F \varphi$ (z is the valency of the ion, F is the Faraday constant, and φ is the local electrostatic potential at the solution-membrane interface) (Bard et al. 1980). Chemical potential, μ_i , can be further expressed by the standard state chemical potential, μ_i^0 , activity of species, a_i , and hydrostatic pressure, P : $\mu_i = \mu_i^0 + R_g T \ln a_i + \bar{V}_i P$ (Callen 1985). Here, R_g is the gas constant, T is the absolute temperature, and \bar{V} is the partial molar volume of i . Thus, the electrochemical potential of species i is

$$\bar{\mu}_i = \mu_i^0 + R_g T \ln a_i + \bar{V}_i P + z_i F \varphi \quad (2)$$

As both ED and RED operate at practically ambient hydraulic pressures, the hydrostatic pressure difference between the membrane and solution phases can be approximated to zero: $P^{\text{m}} - P^{\text{s}} = 0$. By selecting the same standard-state chemical

potential for both phases, $\mu_i^{m,0} = \mu_i^{s,0}$ (Kontturi et al. 2008), Eqs. 1 and 2 combined reduce to just the activity and electrostatic terms:

$$R_g T \ln a_i^m + z_i F \phi^m = R_g T \ln a_i^s + z_i F \phi^s \quad (3)$$

Activity, a , can be replaced with the product of the concentration, and activity coefficient, γ , which is a function of concentration. Here, the concentration is moles of solute per unit volume of solution. However, the membrane matrix comprises both solution and polymer. Multiplying \bar{c}^m , the concentration normalized by unit volume of solution sorbed in the membrane matrix (i.e., excluding the polymer volume) by the volume fraction of water in the IEM, f_w , gives the concentration normalized by total volume of the water-swollen membrane, $c^m = f_w \bar{c}^m$ (i.e., includes volume of solution and polymer). For the co-ions and counterions (subscripts co and ct, respectively), Eq. 3 can be correspondingly rearranged to

$$\frac{\gamma_{co}^m c_{co}^m}{f_w \gamma_{co}^s c_{co}^s} = \exp \left[-\frac{z_{co} F}{R_g T} \Delta \phi_{Donnan} \right] \quad (4a)$$

$$\frac{\gamma_{ct}^m c_{ct}^m}{f_w \gamma_{ct}^s c_{ct}^s} = \exp \left[-\frac{z_{ct} F}{R_g T} \Delta \phi_{Donnan} \right] \quad (4b)$$

The difference in electrostatic potential across the solution-membrane interface, $\phi^m - \phi^s$, is defined as the Donnan potential, $\Delta \phi_{Donnan}$ (Donnan 1911, Galama et al. 2016, Strathmann 2004b).

Equating the Donnan potentials of Eqs. 4a and b yields Eq. 5 after reordering:

$$c_{co}^m = f_w^{1-Z} \left(\gamma_{ct}^s c_{ct}^s \right)^{-Z} \gamma_{co}^s c_{co}^s \left(\gamma_{co}^m \right)^{-1} \left(\gamma_{ct}^m c_{ct}^m \right)^Z \quad (5)$$

where Z is z_{co}/z_{ct} . Counter- and co-ion activity coefficients within the membrane, γ_{ct}^m and γ_{co}^m , respectively, can be predicted using Manning's counterion condensation model, with good agreement with experimental data (Kamcev et al. 2016, Manning 1969):

$$\gamma_{co}^m = \exp \left\{ -\frac{1}{2} Z^2 \left[1 + \nu_{ct} |z_{ct}| \xi (\nu_{co} + \nu_{ct}) \chi \right]^{-1} \right\} \quad (6a)$$

$$\gamma_{ct}^m = \frac{|z_{ct}|^{-1} \xi^{-1} + \nu_{ct} |z_{ct}| \chi}{1 + \nu_{ct} |z_{ct}| \chi} \exp \left\{ -\frac{1}{2} \left[1 + \nu_{ct} |z_{ct}| \xi (\nu_{co} + \nu_{ct}) \chi \right]^{-1} \right\} \quad (6b)$$

with $\chi = |z_{\text{co}}| c_{\text{co}}^{\text{m}} / c_{\text{fix}}^{\text{m}}$ and ξ being the dimensionless linear charge density of the polymer:

$$\xi = \frac{\lambda_{\text{B}}}{b} = \frac{e^2}{4\pi\epsilon_0\epsilon_r k_{\text{B}} T b} \quad (6c)$$

where λ_{B} is the Bjerrum length, b is the distance between fixed charges on the polymer chain, e is the elementary charge, ϵ_0 is the vacuum permittivity, ϵ_r is the solvent dielectric constant, and k_{B} is the Boltzmann constant. Eqs. 6a and b are applicable for $\xi > |z_{\text{ct}}|^{-1}$; this condition is readily satisfied for the high density of fixed charges within an IEM (Kamcev et al. 2017a).

For 1:1 electrolytes, such as NaCl and MgSO₄, $z_{\text{co}} = -z_{\text{ct}}$ and, hence, Z is -1 .

Additionally, substituting in $c_{\text{co}}^{\text{s}} = \nu_{\text{co}} c^{\text{s}}$, $c_{\text{ct}}^{\text{s}} = \nu_{\text{ct}} c^{\text{s}}$, and $\gamma_{\text{co}}^{\text{s}} \gamma_{\text{ct}}^{\text{s}} = (\gamma_{\pm}^{\text{s}})^2$ (Robinson and Stokes 1959) further reduces Eq. 5 to

$$c_{\text{co}}^{\text{m}} = \frac{\nu_{\text{co}} \nu_{\text{ct}} f_{\text{w}}^2 (\gamma_{\pm}^{\text{s}} c^{\text{s}})^2}{\gamma_{\text{co}}^{\text{m}} \gamma_{\text{ct}}^{\text{m}} c_{\text{ct}}^{\text{m}}} \quad (7)$$

where ν is the number of counter- or co-ions each electrolyte molecule dissociates into (i.e., $\nu_{\text{co}} = \nu_{\text{ct}} = 1$ for NaCl). The salt activity coefficient in bulk solution, γ_{\pm}^{s} , can be predicted using theoretical models; in this study, the Pitzer equations are employed for NaCl (Pitzer 1973, Pitzer and Mayorga 1973). Eqs. 1-6 are general equations for all electrolytes, whereas Eq. 7 is specific to 1:1 electrolytes. The equations are applicable for equilibrium at both HC and LC solution-membrane interfaces (Figure A-1).

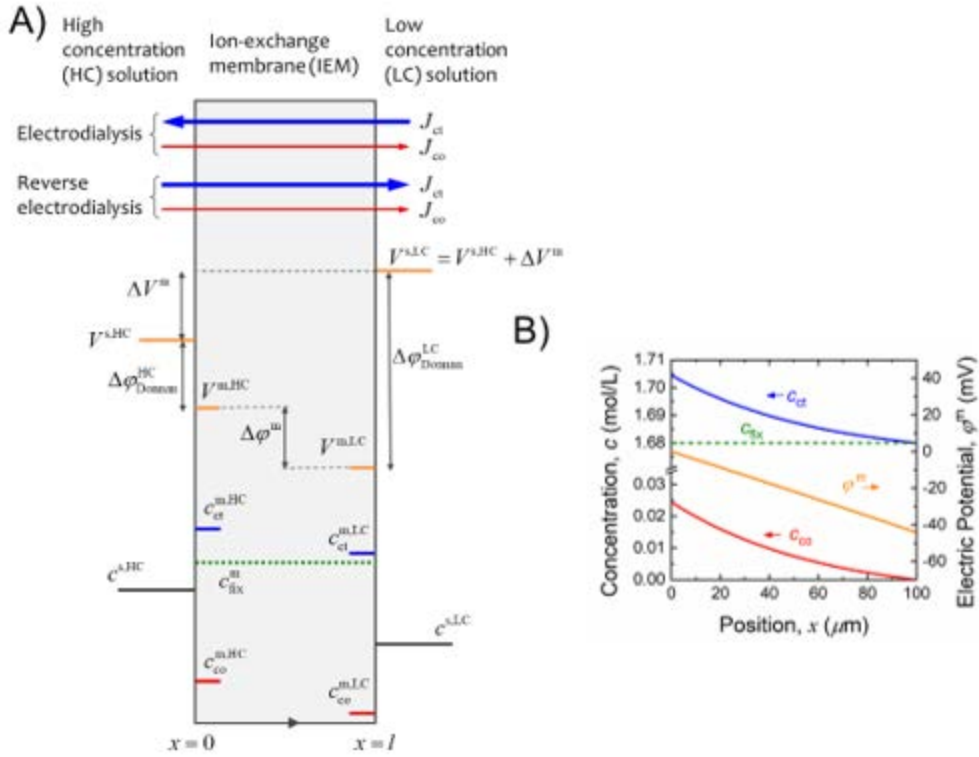


Figure A-1. A) Schematic depicting counter- and co-ion fluxes in IEM process; B) Concentration profiles of counterion, co-ion, and fixed charge within the IEM for an illustrative IEM process.

Besides the condition of electrochemical potential equilibrium between the solution and membrane phases, charge balance also needs to be preserved at all points within the membrane, including the interfaces:

$$|z_{co}|c_{co}^m + c_{fix} = |z_{ct}|c_{ct}^m \quad (8)$$

Rearranging Eq. 8 yields

$$c_{co}^m = \frac{|z_{ct}|c_{ct}^m - c_{fix}}{|z_{co}|} \quad (9)$$

which can be solved simultaneously with Eqs. 5 (general case) or 7 (1:1 electrolytes) to determine c_{co}^m and c_{ct}^m . The counter- and co-ion concentrations at the HC and LC solution-membrane interfaces are indicated in Figure A-1A as $c_{ct}^{m,HC}$, $c_{co}^{m,HC}$, $c_{ct}^{m,LC}$, and $c_{co}^{m,LC}$, respectively. The Donnan potential, $\Delta\phi_{Donnan} = \phi^m - \phi^s$, is calculated using Eq. 4 with the membrane and solution activities, $\gamma_i^m c_i^m$ and $\gamma_i^s c_i^s$, and approximating the activity coefficient of counter- and co-ions in bulk solution to be effectively the same, i.e., $\gamma_{ct}^s = \gamma_{co}^s = \gamma_{\pm}^s$. Indicated in Figure

A-1A are ϕ^s , ϕ^m , and $\Delta\phi_{\text{Donnan}}$ for the HC and LC solution-membrane interfaces. For this study, NaCl, a 1:1 electrolyte, is employed. The effect of pH is negligible, since the contribution of H^+ and OH^- to the electrolyte composition is small ($< 10^{-4}$ mol/L) compared to Na^+ and Cl^- concentrations ($> 10^{-2}$ mol/L) across the environmentally-relevant pHs of 4-10.

Nernst-Planck equation for transport across membrane

During ED separation or RED energy production, a net driving force is present for transport of species across the IEM. At steady state, the molar ion flux is governed by (Helfferich 1962):

$$J_i = -\frac{D_i^m c_i^m}{R_g T} \frac{d\bar{\mu}_i^m}{dx} \quad (10)$$

where D^m is the ion diffusion coefficient and x is the flux direction (i.e., across membrane thickness). The electrochemical potential of counter- or co-ions in the membrane, $\bar{\mu}_i^m$, is described by Eq. 2 and includes the electrical potential and activity terms, $z_i F \phi + R_g T \ln \gamma c$, assuming no hydraulic pressure gradient within the membrane matrix. Substituting the terms into Eq. 10 yields the Nernst-Planck equation (modified to account for activity coefficient):

$$J_i = -D_i^m c_i^m \left(\frac{d \ln(\gamma_i^m c_i^m)}{dx} + \frac{z_i F}{R_g T} \frac{d\phi^m}{dx} \right) \quad (11)$$

The first term of Eq. 11 denotes Fickian diffusion of ions down an activity or, effectively, concentration gradient, whereas the second term signifies migration of the charged species under an electric field within the membrane. Expressions for the local concentration and electric potential gradients within the membrane can be derived by combining Eq. 11 for counter- and co-ions:

$$\frac{dc^m}{dx} = \left(\frac{J_{\text{co}}}{z_{\text{co}} D_{\text{co}}^m c_{\text{co}}^m} - \frac{J_{\text{ct}}}{z_{\text{ct}} D_{\text{ct}}^m c_{\text{ct}}^m} \right) \left(\frac{\beta_{\text{ct}}}{z_{\text{ct}} c_{\text{ct}}^m} - \frac{\beta_{\text{co}}}{z_{\text{co}} c_{\text{co}}^m} \right)^{-1} \quad (12)$$

$$\frac{d\phi^m}{dx} = \frac{R_g T}{F} \left(\frac{J_{\text{co}}}{D_{\text{co}}^m \beta_{\text{co}}^m} - \frac{J_{\text{ct}}}{D_{\text{ct}}^m \beta_{\text{ct}}^m} \right) \left(\frac{z_{\text{ct}} c_{\text{ct}}^m}{\beta_{\text{ct}}} - \frac{z_{\text{co}} c_{\text{co}}^m}{\beta_{\text{co}}} \right)^{-1} \quad (13)$$

where $\beta_i = 1 + c_i^m (d \ln \gamma_i^m / dc_i^m)$. The concentration and electric potential gradients are functions of the ion fluxes and local membrane concentrations. It is instructive to note that because of the electroneutrality constraint, the slopes of counter- and co-ion concentrations are identical and dc^m/dx of Eq. 12 is applicable to both c_{ct} and c_{co} . Summing the two Donnan potentials at the solution-membrane interfaces and the internal electric potential difference within the IEM, $\Delta\phi^m$,

yields the external electric potential difference across the membrane,

$$\Delta V^m = \Delta \varphi^m + \Delta \varphi_{\text{Donnan}}^{\text{HC}} - \Delta \varphi_{\text{Donnan}}^{\text{LC}} \quad (\text{Figure A-1}).$$

Numerical solutions for J_{co} and J_{ct} can be obtained using the finite difference method: the membrane thickness is discretized into one-dimensional finite elements, across which Eqs. 12 and 13 are simultaneously solved to satisfy both charge balance along the entire membrane thickness (i.e., local electroneutrality, Eq. 8) and boundary conditions determined in the preceding section, i.e.,

$$c_i^m = c_i^{\text{m,HC}} \quad \text{and} \quad \varphi^m = \varphi^{\text{m,HC}} \quad \text{at} \quad x = 0, \quad \text{and} \quad c_i^m = c_i^{\text{m,LC}} \quad \text{and} \quad \varphi^m = \varphi^{\text{m,LC}} \quad \text{at} \quad x = l.$$

Python codes are used to converge on the pair of ion fluxes that meets all constraints: the interfacial ion concentrations, $c_i^{\text{m,HC}}$ and $c_i^{\text{m,LC}}$ (which are at equilibrium with external bulk concentrations) and the ΔV^m specified (or the equivalent $\Delta \varphi^m$).

Effective ion diffusivities within the membrane matrix of polymer and sorbed solution account for the lengthened diffusional pathway, i.e., increased tortuosity and fraction of free volume (equivalently, water volume fraction, f_w) < 1 , and are modeled using the lattice approach by multiplying the diffusion coefficient in free space with the factor $f_w^2/(2-f_w)^2$ (Mackie and Meares 1955a, b). The diffusion coefficient of counter- and co-ions under the locally inhomogeneous electric field of a charged ion-exchange membrane can be predicted using the counterion condensation model (Kamcev et al. 2017b, Manning 1969). Incorporating the tortuosity factor and fraction of free volume, D_{co}^m and D_{ct}^m can be described by the following equations:

$$D_{\text{co}}^m = D_{\text{co}}^s \left(\frac{f_w}{2-f_w} \right)^2 \left(1 - \frac{|z_{\text{co}}|^2 A}{3} \right) \quad (14a)$$

$$D_{\text{ct}}^m = D_{\text{ct}}^s \left(\frac{f_w}{2-f_w} \right)^2 \left(\frac{|z_{\text{ct}}|^{-1} \xi^{-1} + \nu_{\text{ct}} |z_{\text{ct}}| \chi}{1 + \nu_{\text{ct}} |z_{\text{ct}}| \chi} \right) \left(1 - \frac{|z_{\text{ct}}|^2 A}{3} \right) \quad (14b)$$

$$A = |z_{\text{ct}}|^{-2} \sum_{m_1=-\infty}^{\infty} \sum_{m_2=-\infty}^{\infty} \left[1 + \pi (m_1^2 + m_2^2) + (\nu_{\text{co}} + \nu_{\text{ct}}) |z_{\text{co}} z_{\text{ct}}| \xi \chi \right]^{-2} \Big|_{(m_1, m_2) \neq (0,0)} \quad (14c)$$

$$\approx |z_{\text{ct}}|^{-2} \left[1 + \pi + (\nu_{\text{co}} + \nu_{\text{ct}}) |z_{\text{co}} z_{\text{ct}}| \xi \chi \right]^{-1}$$

Eqs. 14a-c are applicable for $\xi > |z_{\text{ct}}|^{-1}$. Note that in ED, the counterion flux, J_{ct} , is against the concentration gradient, and the co-ion flux, J_{co} , is in the opposite direction, whereas both J_{ct} and J_{co} are down dc/dx for RED (Figure A-1).

Additionally, the flux of water can be neglected as it is relatively small compared to the ion fluxes (Strathmann 2004b).

The transport model presented here bears analogous similarity to the solution-diffusion transport mechanism across dense nonporous membranes (Paul 2004, Wijmans and Baker 1995), as mentioned in a recent study (Kamcev et al. 2017b). In the solution-diffusion model, species partition or sorb from the bulk solution into the membrane at the interface and $c_i^m/c_i^s = K_i$ where K_i is the partition coefficient. Correspondingly, in IEM transport, the distribution of ion concentrations in the solution and membrane at the interface is governed by the Donnan potential, Eqs. 4a and 4b, and the equivalent partition coefficient is $K_i = f_w \gamma_i^s \exp[-z_i F \Delta \phi_{\text{Donnan}} / R_g T] / \gamma_i^m$. Species diffuse across the dense membrane driven by a chemical potential gradient in the solution-diffusion mechanism. This is paralleled by species transport under an electrochemical potential across the ion-exchange membrane in ED and RED.

Performance parameters for ED and RED

Current efficiency

Current efficiency, CE, is a measure of ionic current use in ED and RED for separation and energy production, respectively:

$$CE_{\text{ED}} = \frac{z_{\text{ct}} J_{\text{ct}}}{z_{\text{co}} J_{\text{co}} + z_{\text{ct}} J_{\text{ct}}} \quad (15a)$$

$$CE_{\text{RED}} = \frac{z_{\text{co}} J_{\text{co}} + z_{\text{ct}} J_{\text{ct}}}{z_{\text{ct}} J_{\text{ct}}} \quad (15b)$$

where z is the ion valence, J is the ion flux, and subscripts ct and co denote counter- and co-ions, respectively. Note that z and J can be positive or negative, depending on charge and direction, and the product zJ gives the ionic current. In ED desalination, the electric current drives counter- and co-ion fluxes. These two ion fluxes flow in opposite directions and are of different charge, with only the counterion flux performing the desired function of desalinating the saline feed, whereas co-ion flux is an unwanted leakage of ions to the diluate stream that actually compromise desalination performance. Current efficiency for ED desalination is, thus, the ratio of the current due to counterion flux to the total ionic current, Eq. 15a. Conversely, the aim of RED is to generate an ion flux that can then be used to drive an external circuit and, hence, CE_{RED} is defined differently from ED desalination. Because both fluxes are in the same direction, the current from counterion flux is partly negated by co-ion flux. The RED current efficiency, Eq. 15b, is the net ionic current divided by the current due to counterion flux. Note that equation for CE_{RED} is the reciprocal of CE_{ED} . Current efficiency of ED and RED is analogous to the Faradaic efficiency of electrochemical processes, which quantifies the percentage of charge used for the desired electrochemical reaction.

Permselectivity

Permselectivity, α , describes the selectivity for counterion transport and is defined as the ionic current carried by counterion flux less the current from co-ion flux, normalized by the total ionic current (Sata 2007, Strathmann 2004b):

$$\alpha = \frac{|z_{ct}J_{ct}| - |z_{co}J_{co}|}{\sum |z_i J_i|} = t_{ct} - t_{co} \quad (16)$$

Note that the sign conventions of z and J are neglected and only the magnitude of the ionic currents are used to calculate α . Further, the fraction of total ionic current carried by species i is the transport number, t_i , and, hence, permselectivity is also the counterion transport number less the co-ion transport number (Eq. 16) (Strathmann 2004b). An IEM with perfect charge selectivity is only permeable to counterions but not co-ions and, therefore, permselectivity equals to one.

Experimentally characterized α measurements are commonly reported in literature, but those values are more accurately termed “apparent permselectivity,” α_{app} , and is the ratio of measured open-circuit voltage to theoretical Nernst potential (Strathmann 2004b). Because of the ease of experimental characterization (one electrochemical reading instead of tracking counter- and co-ion concentration changes), apparent permselectivity is often used as a proxy parameter to approximate the fraction of ionic current carried by counter- and co-ions during actual ED and RED operation, even though it deviates from the definition of Eq. 16.

Area specific resistance

Area specific resistance, ASR, is defined in Eq. 17 as the slope of ΔV^m with respect to the net current density, $\hat{i}_{tot} = F(z_{co}J_{co} + z_{ct}J_{ct})$ (i.e., differential resistance):

$$ASR = \frac{d\Delta V^m}{d\hat{i}_{tot}} \quad (17)$$

Because the contribution of IEM to total internal resistance is significant in ED and RED (Yip et al. 2014), the membrane ASR should be small to suppress undesired resistive losses. In IEM processes, steady state current-voltage response can be described by one of the three regimes: ohmic (or under-limiting), plateau (or limiting), and overlimiting (Rosenberg and Tirrell 1957). The current analysis will focus on simulating IEMs working within the ohmic regime, which is the common operating conditions for ED and RED. In this relatively low current regime (i.e., under-limiting the relation between current density and imposed voltage is linear), ion depletion in the concentration polarization boundary layer is not dominant and a limiting current is not reached (i.e., before plateau regime).

Conductivity

Conductivity, σ , is the reciprocal of resistivity, ρ , and describes the ability of the IEM to conduct ionic currents:

$$\sigma = \text{ASC} \times l = \rho^{-1} \quad (18)$$

where ASC is the area specific conductance of membrane, which is equal to the multiplicative inverse of ASR, and l is the ion-exchange membrane thickness. It is instructive to note that conductivity and resistivity are intensive properties (i.e., independent of membrane physical dimensions), whereas ASC and ASR are extensive properties. Introducing σ and ASC enables the relationship between conductivity and permselectivity to be examined in an analytical framework akin to permeability-selectivity of gas separation and salt-rejecting membranes (Freeman 1999, Park et al. 2017).

References

- Baker, R.W. (2012) Membrane technology and applications, John Wiley & Sons, Chichester, West Sussex ; Hoboken.
- Bard, A.J., Faulkner, L.R., Leddy, J. and Zoski, C.G. (1980) Electrochemical methods: fundamentals and applications, Wiley New York.
- Bogardi, J.J., Dudgeon, D., Lawford, R., Flinkerbusch, E., Meyn, A., Pahl-Wostl, C., Vielhauer, K. and Vörösmarty, C. (2012) Water security for a planet under pressure: interconnected challenges of a changing world call for sustainable solutions. *Current Opinion in Environmental Sustainability* 4(1), 35-43.
- Callen, H.B. (1985) Thermodynamics and an Introduction to Thermostatistics, Wiley.
- Cho, D.H., Lee, K.H., Kim, Y.M., Park, S.H., Lee, W.H., Lee, S.M. and Lee, Y.M. (2017) Effect of cationic groups in poly(arylene ether sulfone) membranes on reverse electro dialysis performance. *Chemical Communications* 53(15), 2323-2326.
- Cooley, H., Donnelly, K., Ross, N. and Luu, P. (2012) Proposed seawater desalination facilities in California.
- Cui, W., Kerres, J. and Eigenberger, G. (1998) Development and characterization of ion-exchange polymer blend membranes. *Separation and Purification Technology* 14(1-3), 145-154.
- Daniilidis, A., Vermaas, D.A., Herber, R. and Nijmeijer, K. (2014) Experimentally obtainable energy from mixing river water, seawater or brines with reverse electro dialysis. *Renewable Energy* 64, 123-131.
- Długołęcki, P., Nijmeijer, K., Metz, S. and Wessling, M. (2008a) Current status of ion exchange membranes for power generation from salinity gradients. *Journal of Membrane Science* 319(1-2), 214-222.
- Długołęcki, P., Nijmeijer, K., Metz, S. and Wessling, M. (2008b) Current status of ion exchange membranes for power generation from salinity gradients. *Journal of Membrane Science* 319(1-2), 214-222.
- Donnan, F.G. (1911) Theorie der Membrangleichgewichte und Membranpotentiale bei Vorhandensein von nicht dialysierenden Elektrolyten. Ein Beitrag zur physikalisch - chemischen Physiologie. *Berichte der Bunsengesellschaft für physikalische Chemie* 17(14), 572-581.

- Elimelech, M. (2006) Special Paper: The global challenge for adequate and safe water. *Journal of Water Supply: Research & Technology-AQUA* 55(1), 3-10.
- Elimelech, M. and Phillip, W.A. (2011) The Future of Seawater Desalination: Energy, Technology, and the Environment. *Science* 333(6043), 712-717.
- Freeman, B.D. (1999) Basis of permeability/selectivity trade-off relations in polymeric gas separation membranes. *Macromolecules* 32(2), 375-380.
- Galama, A., Post, J., Hamelers, H., Nikonenko, V. and Biesheuvel, P. (2016) On the origin of the membrane potential arising across densely charged ion exchange membranes: How well does the Teorell-Meyer-Sievers theory work? *Journal of Membrane Science and Research* 2(3), 128-140.
- Galama, A.H., Vermaas, D.A., Veerman, J., Saakes, M., Rijnaarts, H.H.M., Post, J.W. and Nijmeijer, K. (2014) Membrane resistance: The effect of salinity gradients over a cation exchange membrane. *Journal of Membrane Science* 467, 279-291.
- Geise, G.M., Curtis, A.J., Hatzell, M.C., Hickner, M.A. and Logan, B.E. (2014a) Salt Concentration Differences Alter Membrane Resistance in Reverse Electrodialysis Stacks. *Environmental Science & Technology Letters* 1(1), 36-39.
- Geise, G.M., Hickner, M.A. and Logan, B.E. (2013) Ionic resistance and permselectivity trade-offs in anion exchange membranes. *Acs Applied Materials & Interfaces* 5(20), 10294-10301.
- Geise, G.M., Paul, D.R. and Freeman, B.D. (2014b) Fundamental water and salt transport properties of polymeric materials. *Progress in Polymer Science* 39(1), 1-42.
- Ghaffour, N., Missimer, T.M. and Amy, G.L. (2013) Technical review and evaluation of the economics of water desalination: Current and future challenges for better water supply sustainability. *Desalination* 309, 197-207.
- Gleick, P.H. (2010) Roadmap for sustainable water resources in southwestern North America. *Proceedings of the National Academy of Sciences* 107(50), 21300-21305.
- Gromov, A., Dittmer, S., Svensson, J., Nerushev, O.A., Perez-García, S.A., Licea-Jiménez, L., Rychwalski, R. and Campbell, E.E. (2005) Covalent amino-functionalisation of single-wall carbon nanotubes. *Journal of Materials Chemistry* 15(32), 3334-3339.
- Guler, E., Elizen, R., Vermaas, D.A., Saakes, M. and Nijmeijer, K. (2013) Performance-determining membrane properties in reverse electrodialysis. *Journal of Membrane Science* 446, 266-276.

- Güler, E., Elizen, R., Vermaas, D.A., Saakes, M. and Nijmeijer, K. (2013) Performance-determining membrane properties in reverse electrodialysis. *Journal of Membrane Science* 446, 266-276.
- Guler, E., Zhang, Y., Saakes, M. and Nijmeijer, K. (2012) Tailor - made anion - exchange membranes for salinity gradient power generation using reverse electrodialysis. *ChemSusChem* 5(11), 2262-2270.
- Hamon, M.A., Chen, J., Hu, H., Chen, Y., Itkis, M.E., Rao, A.M., Eklund, P.C. and Haddon, R.C. (1999) Dissolution of single - walled carbon nanotubes. *Advanced Materials* 11(10), 834-840.
- He, G., Li, Z., Zhao, J., Wang, S., Wu, H., Guiver, M.D. and Jiang, Z. (2015) Nanostructured Ion - Exchange Membranes for Fuel Cells: Recent Advances and Perspectives. *Advanced Materials* 27(36), 5280-5295.
- Helfferrich, F.G. (1962) Ion exchange, Courier Corporation.
- Hong, J.G., Zhang, B.P., Glabman, S., Uzal, N., Dou, X.M., Zhang, H.G., Wei, X.Z. and Chen, Y.S. (2015) Potential ion exchange membranes and system performance in reverse electrodialysis for power generation: A review. *Journal of Membrane Science* 486, 71-88.
- Hwang, G.J., Ohya, H. and Nagai, T. (1999) Ion exchange membrane based on block copolymers. Part III: preparation of cation exchange membrane. *Journal of Membrane Science* 156(1), 61-65.
- Jiang, G., Wang, L., Chen, C., Dong, X., Chen, T. and Yu, H. (2005) Study on attachment of highly branched molecules onto multiwalled carbon nanotubes. *Materials Letters* 59(16), 2085-2089.
- Kamcev, J., Galizia, M., Benedetti, F.M., Jang, E.S., Paul, D.R., Freeman, B.D. and Manning, G.S. (2016) Partitioning of mobile ions between ion exchange polymers and aqueous salt solutions: importance of counter-ion condensation. *Physical Chemistry Chemical Physics* 18(8), 6021-6031.
- Kamcev, J., Paul, D.R. and Freeman, B.D. (2017a) Effect of fixed charge group concentration on equilibrium ion sorption in ion exchange membranes. *Journal of Materials Chemistry A* 5(9), 4638-4650.
- Kamcev, J., Paul, D.R., Manning, G.S. and Freeman, B.D. (2017b) Predicting Salt Permeability Coefficients in Highly Swollen, Highly Charged Ion Exchange Membranes. *Acs Applied Materials & Interfaces* 9(4), 4044-4056.
- Kamcev, J., Sujanani, R., Jang, E.S., Yan, N., Moe, N., Paul, D.R. and Freeman, B.D. (2018) Salt concentration dependence of ionic conductivity in ion exchange membranes. *Journal of Membrane Science* 547, 123-133.

- Kariduraganavar, M., Nagarale, R., Kittur, A. and Kulkarni, S. (2006) Ion-exchange membranes: preparative methods for electrodialysis and fuel cell applications. *Desalination* 197(1-3), 225-246.
- Kontturi, K., Murtomäki, L. and Manzanares, J.A. (2008) *Ionic Transport Processes: In Electrochemistry and Membrane Science*, Oxford University Press.
- Lindstrand, V., Sundström, G. and Jönsson, A.-S. (2000) Fouling of electrodialysis membranes by organic substances. *Desalination* 128(1), 91-102.
- MacDonald, G.M. (2010) Water, climate change, and sustainability in the southwest. *Proceedings of the National Academy of Sciences* 107(50), 21256-21262.
- Mackie, J.S. and Meares, P. (1955a) The Diffusion of Electrolytes in a Cation-Exchange Resin Membrane .1. Theoretical. *Proceedings of the Royal Society of London Series a-Mathematical and Physical Sciences* 232(1191), 498-509.
- Mackie, J.S. and Meares, P. (1955b) The Diffusion of Electrolytes in a Cation-Exchange Resin Membrane .2. Experimental. *Proceedings of the Royal Society of London Series a-Mathematical and Physical Sciences* 232(1191), 510-518.
- Manning, G.S. (1969) Limiting laws and counterion condensation in polyelectrolyte solutions II. Self - diffusion of the small ions. *The Journal of Chemical Physics* 51(3), 934-938.
- Mondor, M., Masse, L., Ippersiel, D., Lamarche, F. and Massé, D.I. (2008) Use of electrodialysis and reverse osmosis for the recovery and concentration of ammonia from swine manure. *Bioresource Technology* 99(15), 7363-7368.
- Moulder, J., Stickle, W., Sobol, P. and Bomben, K. *Handbook of X-Ray Photoelectron Spectroscopy* (Perkin-Elmer Corporation, Physical Electronics Division: Eden Prairie, MN,(1992). There is no corresponding record for this reference.
- Mulder, M. (1996) *Basic principles of membrane technology*, Kluwer Academic, Dordrecht ; Boston.
- Nagarale, R.K., Gohil, G.S. and Shahi, V.K. (2006) Recent developments on ion-exchange membranes and electro-membrane processes. *Advances in Colloid and Interface Science* 119(2-3), 97-130.
- Oki, T. and Kanae, S. (2006) Global Hydrological Cycles and World Water Resources. *Science* 313(5790), 1068-1072.

- Park, H.B., Kamcev, J., Robeson, L.M., Elimelech, M. and Freeman, B.D. (2017) Maximizing the right stuff: The trade-off between membrane permeability and selectivity. *Science* 356(6343).
- Paul, D.R. (2004) Reformulation of the solution-diffusion theory of reverse osmosis. *Journal of Membrane Science* 241(2), 371-386.
- Perry, W., Broers, A., El-Baz, F., Harris, W., Healy, B. and Hillis, W.D. (2008) Grand challenges for engineering. National Academy of Engineering, Washington, DC.
- Pitzer, K.S. (1973) Thermodynamics of electrolytes. I. Theoretical basis and general equations. *The Journal of Physical Chemistry* 77(2), 268-277.
- Pitzer, K.S. and Mayorga, G. (1973) Thermodynamics of electrolytes. II. Activity and osmotic coefficients for strong electrolytes with one or both ions univalent. *The Journal of Physical Chemistry* 77(19), 2300-2308.
- Ran, J., Wu, L., He, Y.B., Yang, Z.J., Wang, Y.M., Jiang, C.X., Ge, L., Bakangura, E. and Xu, T.W. (2017) Ion exchange membranes: New developments and applications. *Journal of Membrane Science* 522, 267-291.
- Robinson, R.A. and Stokes, R.H. (1959) *Electrolyte Solutions ... Second edition*, Butterworths Scientific Publications, London.
- Rockström, J., Steffen, W., Noone, K., Persson, Å., Chapin III, F.S., Lambin, E.F., Lenton, T.M., Scheffer, M., Folke, C. and Schellnhuber, H.J. (2009) A safe operating space for humanity. *nature* 461(7263), 472.
- Rosenberg, N. and Tirrell, C. (1957) Limiting currents in membrane cells. *Industrial & Engineering Chemistry* 49(4), 780-784.
- Running, S.W. (2012) A Measurable Planetary Boundary for the Biosphere. *Science* 337(6101), 1458-1459.
- Sabo, J.L., Sinha, T., Bowling, L.C., Schoups, G.H.W., Wallender, W.W., Campana, M.E., Cherkauer, K.A., Fuller, P.L., Graf, W.L., Hopmans, J.W., Kominoski, J.S., Taylor, C., Trimble, S.W., Webb, R.H. and Wohl, E.E. (2010) Reclaiming freshwater sustainability in the Cadillac Desert. *Proceedings of the National Academy of Sciences* 107(50), 21263-21269.
- Sadrzadeh, M. and Mohammadi, T. (2008) Sea water desalination using electrodialysis. *Desalination* 221(1-3), 440-447.
- Sata, T. (2004) *Ion exchange membranes : preparation, characterization, modification and application*, Royal Society of Chemistry, Cambridge.
- Sata, T. (2007) *Ion exchange membranes: preparation, characterization, modification and application*, Royal Society of chemistry.

- Shannon, M.A., Bohn, P.W., Elimelech, M., Georgiadis, J.G., Marinas, B.J. and Mayes, A.M. (2008) Science and technology for water purification in the coming decades. *Nature* 452(7185), 301-310.
- Strathmann, H. (2004a) Ion-exchange membrane separation processes, Elsevier, Amsterdam ; Boston.
- Strathmann, H. (2004b) Ion-exchange membrane separation processes, Elsevier.
- Strathmann, H. (2010) Electrodialysis, a mature technology with a multitude of new applications. *Desalination* 264(3), 268-288.
- Takamuku, S., Wohlfarth, A., Manhart, A., Rader, P. and Jannasch, P. (2015) Hypersulfonated polyelectrolytes: preparation, stability and conductivity. *Polymer Chemistry* 6(8), 1267-1274.
- Tanaka, Y. (2015) Ion Exchange Membranes (Second Edition), Elsevier, Amsterdam.
- Tanghe, L.J. and Brewer, R.J. (1968) Equilibrium between sulfuric and acetylsulfuric acids in acetic acid-acetic anhydride. *Analytical Chemistry* 40(2), 350-353.
- Tedesco, M., Brauns, E., Cipollina, A., Micale, G., Modica, P., Russo, G. and Helsen, J. (2015a) Reverse electrodialysis with saline waters and concentrated brines: a laboratory investigation towards technology scale-up. *Journal of Membrane Science* 492, 9-20.
- Tedesco, M., Cipollina, A., Tamburini, A. and Micale, G. (2017) Towards 1 kW power production in a reverse electrodialysis pilot plant with saline waters and concentrated brines. *Journal of Membrane Science* 522, 226-236.
- Tedesco, M., Cipollina, A., Tamburini, A., Micale, G., Helsen, J. and Papapetrou, M. (2015b) REAPower: use of desalination brine for power production through reverse electrodialysis. *Desalination and Water Treatment* 53(12), 3161-3169.
- Tedesco, M., Hamelers, H.V.M. and Biesheuvel, P.M. (2018) Nernst-Planck transport theory for (reverse) electrodialysis: III. Optimal membrane thickness for enhanced process performance. *Journal of Membrane Science* 565, 480-487.
- Tedesco, M., Scalici, C., Vaccari, D., Cipollina, A., Tamburini, A. and Micale, G. (2016) Performance of the first reverse electrodialysis pilot plant for power production from saline waters and concentrated brines. *Journal of Membrane Science* 500, 33-45.
- Toomey, R., Freidank, D. and Ruhe, J. (2004) Swelling behavior of thin, surface-attached polymer networks. *Macromolecules* 37(3), 882-887.

- van der Hoek, J.P., Rijnbende, D.O., Lokin, C.J.A., Bonn , P.A.C., Loonen, M.T. and Hofman, J.A.M.H. (1998) Electrodialysis as an alternative for reverse osmosis in an integrated membrane system. *Desalination* 117(1-3), 159-172.
- Vardner, J.T., Ling, T., Russell, S.T., Perakis, A.M., He, Y., Brady, N.W., Kumar, S.K. and West, A.C. (2017) Method of Measuring Salt Transference Numbers in Ion-Selective Membranes. *Journal of The Electrochemical Society* 164(13), A2940-A2947.
- Vorosmarty, C.J., McIntyre, P.B., Gessner, M.O., Dudgeon, D., Prusevich, A., Green, P., Glidden, S., Bunn, S.E., Sullivan, C.A., Liermann, C.R. and Davies, P.M. (2010) Global threats to human water security and river biodiversity. *Nature* 467(7315), 555-561.
- Wang, G.G., Weng, Y.M., Chu, D., Chen, R.R. and Xie, D. (2009) Developing a polysulfone-based alkaline anion exchange membrane for improved ionic conductivity. *Journal of Membrane Science* 332(1-2), 63-68.
- Wang, Y., Iqbal, Z. and Malhotra, S.V. (2005) Functionalization of carbon nanotubes with amines and enzymes. *Chemical physics letters* 402(1-3), 96-101.
- Wei, Y., Ling, X., Zou, L., Lai, D., Lu, H. and Xu, Y. (2015) A facile approach toward preparation of sulfonated multi-walled carbon nanotubes and their dispersibility in various solvents. *Colloids and Surfaces A: Physicochemical and Engineering Aspects* 482, 507-513.
- Wijmans, J.G. and Baker, R.W. (1995) The solution-diffusion model: a review. *Journal of Membrane Science* 107(1-2), 1-21.
- Xu, T. (2005a) Ion exchange membranes: state of their development and perspective. *Journal of Membrane Science* 263(1-2), 1-29.
- Xu, T. (2005b) Ion exchange membranes: State of their development and perspective. *Journal of Membrane Science* 263(1-2), 1-29.
- Yip, N.Y., Brogioli, D., Hamelers, H.V.M. and Nijmeijer, K. (2016) Salinity Gradients for Sustainable Energy: Primer, Progress, and Prospects. *Environmental Science & Technology* 50(22), 12072-12094.
- Yip, N.Y., Vermaas, D.A., Nijmeijer, K. and Elimelech, M. (2014) Thermodynamic, Energy Efficiency, and Power Density Analysis of Reverse Electrodialysis Power Generation with Natural Salinity Gradients. *Environmental Science & Technology* 48(9), 4925-4936.
- Younos, T. (2005) The Economics of Desalination. *Journal of Contemporary Water Research & Education* 132(1), 39-45.

- Yun, S., Im, H., Heo, Y. and Kim, J. (2011) Crosslinked sulfonated poly (vinyl alcohol)/sulfonated multi-walled carbon nanotubes nanocomposite membranes for direct methanol fuel cells. *Journal of membrane science* 380(1-2), 208-215.
- Zhang, L., Wang, X.-j., Wang, J., Grinberg, N., Krishnamurthy, D. and Senanayake, C.H. (2009) An improved method of amide synthesis using acyl chlorides. *Tetrahedron Letters* 50(24), 2964-2966.
- Zhang, Y., Desmidt, E., Van Looveren, A., Pinoy, L., Meessaert, B. and Van der Bruggen, B. (2013) Phosphate Separation and Recovery from Wastewater by Novel Electrodialysis. *Environmental Science & Technology* 47(11), 5888-5895.